Dalton Transactions

PAPER

View Article Online
View Journal

Cite this: DOI: 10.1039/c5dt04788a

Synthesis, characterization, DNA binding, cleavage activity, cytotoxicity and molecular docking of new nano water-soluble [M(5-CH_2PPh_3-3,4-salpyr)]$(ClO_4)_2$ (M = Ni, Zn) complexes†

Zeinab Mandegani,[a] Zahra Asadi,*[a] Mozaffar Asadi,[a] Hamid Reza Karbalaei-Heidari[b] and Banafsheh Rastegari[b]

Received 8th December 2015,
Accepted 25th February 2016

DOI: 10.1039/c5dt04788a

www.rsc.org/dalton

Some new water soluble complexes [*N*,*N*′-bis{5-[(triphenyl phosphonium chloride)-methyl]salicylidine}-3,4-diaminopyridine] M(II), which are formulated as nano-[Zn(5-CH_2PPh_3-3,4-salpyr)]$(ClO_4)_2$ (**1**), [Zn(5-CH_2PPh_3-3,4-salpyr)]$(ClO_4)_2$ (**2**), nano-[Ni(5-CH_2PPh_3-3,4-salpyr)]$(ClO_4)_2$ (**3**), [Ni(5-CH_2PPh_3-3,4-salpyr)]$(ClO_4)_2$ (**4**), and [*N*,*N*′-bis{5-[(triphenyl phosphonium chloride)-methyl]salicylidine}-2,3-diaminopyridine]Ni(II)[Ni(5-CH_2PPh_3-2,3-salpyr)]$(ClO_4)_2$ (**5**) have been isolated and characterized by elemental analysis, FT-IR, ^{1}H NMR, ^{13}C NMR, ^{31}P NMR, and UV-vis spectroscopy. The morphology and size of the nano complexes were determined using FE-SEM and TEM. *In vitro* DNA binding studies were investigated by UV-vis absorption spectroscopy, viscosity measurements, CD spectroscopy, cyclic voltammetry, emission spectra and gel electrophoresis, which suggest that the metal complexes act as efficient DNA binders. The absorption spectroscopy of the compounds with DNA reveals that the DNA binding affinity (K_b) has this order: **3** > **4** > **5** > **1** > **2** > **Ligand**. The metal complexes show DNA binding stronger than the ligand, which is expected due to the nature of the metal. The nano complexes display DNA binding stronger than the other complexes which is related to the effect of size on binding affinity and the Ni(II) complexes reveal DNA binding stronger than the corresponding Zn(II) analogues, which is expected due to their *z** effect and geometry. The prominent double strand DNA cleavage abilities of compound **3** are observed in the absence of H_2O_2 with efficiencies of more than 50% even at 70 μM complex concentration. Surprisingly, Zn(II) complexes (compounds **1** & **2**) exhibit a higher cytotoxicity (IC_{50}: 7.3 & 10.9 μM at 24 h; IC_{50}: 4.6 & 8.7 μM at 48 h) against human hepatoma (HepG2) and HeLa cell lines than the Ni(II) complexes (compounds **3**, **4** & **5**) and 5-fluorouracil as control in spite of their inability to cleave DNA. Finally, DNA binding interactions were performed by docking studies. Density functional theory (DFT) studies were performed using the GAUSSIAN 03 program. The DFT method with B3LYP functional, LANL2DZ basis set for metal centers and 6-311g* for other atoms was used. The synthesized compounds and DNA were simulated by molecular docking to explore more details of the ligands conformation and their orientations in the active site of the receptor.

Introduction

The interactions between small molecular ligands and deoxyribonucleic acid (DNA) are of great importance in biology and medicine, due to their essential roles in biochemical, biological and medicinal processes. Meanwhile, DNA remains a biological target of great interest for the design of therapeutic drugs and indicative agents. The capability to interact with DNA has been determined by numerous factors for example coordination geometry and the nature of the ligand. Additional necessary requisites that such complexes should obviously retain are to be stable and inert in the biological environment and being water-soluble. Usually, water solubility has been increased by functionalizing the ligand by charged or polar groups.[1–11]

Currently one of the few most widely used antitumor drugs is cisplatin for treating certain human cancers with incredible success but the development of drug resistance and the dose-limiting nephrotoxicity prevent its potential efficiency.[12,13] So, there is significant attention focused on the design of new metal based anticancer drugs that display improved selectivity and novel modes of DNA interaction similar to non-covalent

[a]*Department of Chemistry, Faculty of Sciences, Shiraz University, Shiraz 71454, Iran. E-mail: Zasadi@shirazu.ac.ir*
[b]*Molecular Biotechnology Laboratory, Department of Biology, Faculty of Sciences, Shiraz University, PO Box 71467–13565, Shiraz 71454, Iran*
†Electronic supplementary information (ESI) available. See DOI: 10.1039/c5dt04788a

interactions that mimic the mode of interaction of biomolecules.[14]

Transition metal complexes that include multi dentate aromatic ligands, with square planar N_4 or N_2O_2 coordination, have some suitable biological properties.[15–20]

Nickel(II)[21] and zinc(II)[22–24] have a variety of biological activities. Ni(II) complexes have shown antibacterial,[25,26] antifungal,[27] antimicrobial[28] and anticancer/antiproliferative[29–31] activities and the zinc complex is utilized for the treatment of Alzheimer disease,[32,33] and can act as radioprotective agents,[34] tumor photosensitizers,[35] anticonvulsants,[36,37] antidiabetic insulin-mimetics,[38–40] anti-inflammatories[41,42] and show cytotoxicity against human cancer cell lines.[43,44]

The application of nanoparticles (NPs) for biomedical usage is usual in the literature and continues to be a rapidly growing research field, with great emphasis on imaging and drug delivery.[45–48] The unique properties of NP based systems give strategic advantages over genuine molecular therapeutics,[49] but new complexities must be examined to make NP based applications a practical option in the clinic. Nanoparticles (NPs), as a subgroup of nanomaterials (NMs), may be determined as particles with all three external dimensions in the range 1–100 nm although, variations on this definition exist.[50] The special physicochemical properties of NMs are suitable for a wide range of applications and due to their small size and structure offer novel capabilities to these materials.[51–57] The development of NMs is also motivated by the confidence that these chemicals will deliver enhanced performances and new functionalities leading, *e.g.*, to smart drugs and assisting in achieving sustainable development, *e.g.*, by reducing the consumption of energy and materials and reducing environmental pollution.[58]

Information about the mode and range of binding of metal center complexes to DNA is important for understanding the cleavage properties of metal complexes. Transition metal complexes are known to bind to DNA *via* both covalent and/or non-covalent interactions. In the covalent binding mode a labile ligand of the complex can be exchanged by a nitrogen base of DNA such as guanine N7, while the non-covalent DNA interactions include intercalative, electrostatic and groove binding of a metal complex outside of the DNA helix, along the major or minor groove.[59,60]

So in the DNA molecule some types of sites bind such as: (i) between two base pairs, (ii) in the minor groove, (iii) in the major groove, and (iv) on the outside of the helix. The interaction advantages depend on the structure of DNA-interacting molecules and the nature of DNA. Small changes in the structure of a DNA-interacting molecule may influence the binding types and stability of the molecule/DNA complex.[61]

Taking into consideration the biological role of nickel and zinc and the fact that metal complexes with drugs may exhibit more pronounced biological properties in comparison with free metal complexes, herein, we report the synthesis of the novel water soluble Ni(II) and Zn(II) complexes with the ligand [*N*,*N*′-bis{5-[(triphenyl phosphonium chloride)-methyl]salicylidine}-3,4-diaminopyridine] (Scheme 1). The final product, $[M(5\text{-}CH_2PPh_3\text{-}3,4\text{-salpyr})](ClO_4)_2$ (M = Zn **1**, **2** and Ni **3**, **4**) and $[Ni(5\text{-}CH_2PPh_3\text{-}2,3\text{-salpyr})](ClO_4)_2$ (**5**) were synthesized that the complexes **1** and **3** were synthesized with nano size . The complexes have been fully characterized by various physicochemical techniques, namely, elemental analyses, spectral (FT-IR, ^1H, ^{13}C ,^{31}P NMR, UV/vis) and cyclic voltammetry (CV). The binding properties of the complexes with fish DNA under physiological conditions have been studied using UV-Vis spectrophotometry, DNA viscosity measurements, cyclic voltammetry (CV), circular dichroism (CD), fluorescence spectroscopy, agarose gel electrophoresis, anticancer activities of the complexes and molecular docking. The Ni(II) complexes (**3–5**) show DNA binding affinities higher than the Zn(II) complexes (**1**, **2**) and interestingly, complex **3** is higher than complex **5**. The nano-sized complexes **1** and **3** display DNA binding stronger than complexes **2** and **4** which are not nano-sized.

It is remarkable that all the complexes display cytotoxicity against human hepatoma (HepG2) and cervical cancer (HeLa) cell lines higher than the currently used chemotherapeutic agent, 5-fluorouracil. The Zn(II) complexes exhibit higher cytotoxicity than their Ni(II) analogues in spite of their inability to cleave DNA. Also, both **1** & **3** are remarkable in killing the cancer cell lines and are more efficient than the classical complexes **2** & **4** through apoptosis which suggests the importance of the nano-sized form of the complexes.

Experimental section

Materials

Zinc(II) acetate dihydrate, nickel(II) acetate tetrahydrate, 2,3-diaminopyridine, 3,4-diaminopyridine, salicylaldehyde, triphenylphosphine, sodium perchlorate, paraformaldehyde, conc. HCl, 0.5% $NaHCO_3$ solution, acetonitrile, ethanol, methanol, deuterated dimethyl sulfoxide (DMSO-d_6), ethylene diamine tetra acetic acid (EDTA), 3-chloroacetylacetone, ammonium acetate and potassium bromide (KBr) were purchased from Merck, Fluka, Acros and Aldrich.

Agarose powder was purchased from Invitrogen. Fish deoxyribonucleic acid was obtained from New England Biolabs (Beijing) Ltd. Tris-HCl-NaCl buffer solution (TBS, 1 mM Tris, 5 mM NaCl, pH 7.2) was used for FS-DNA binding experiments and TAE buffer (40 mM Tris, 20 mM acetic acid, 1 mM EDTA, pH 8.0) was used for the gel electrophoresis experiments. All reagents were used as received and solvents were purified by the standard methods.

Double distilled deionized water was used to prepare buffers, and the ionic strength in buffers was adjusted with NaCl. The DNA concentration in base pairs was determined using an extinction coefficient of 6600 M^{-1} cm^{-1} at 260 nm. The ratio A_{260}/A_{280} > 1.80 was used to indicate high DNA purity. The DNA solution was stored for a short period of time at 4 °C if not used immediately.

Methods and instrumentations

The ^1H NMR and ^{13}C NMR spectra in DMSO-d_6 were recorded on a Bruker Avance DPX 250 spectrometer (with TMS as the

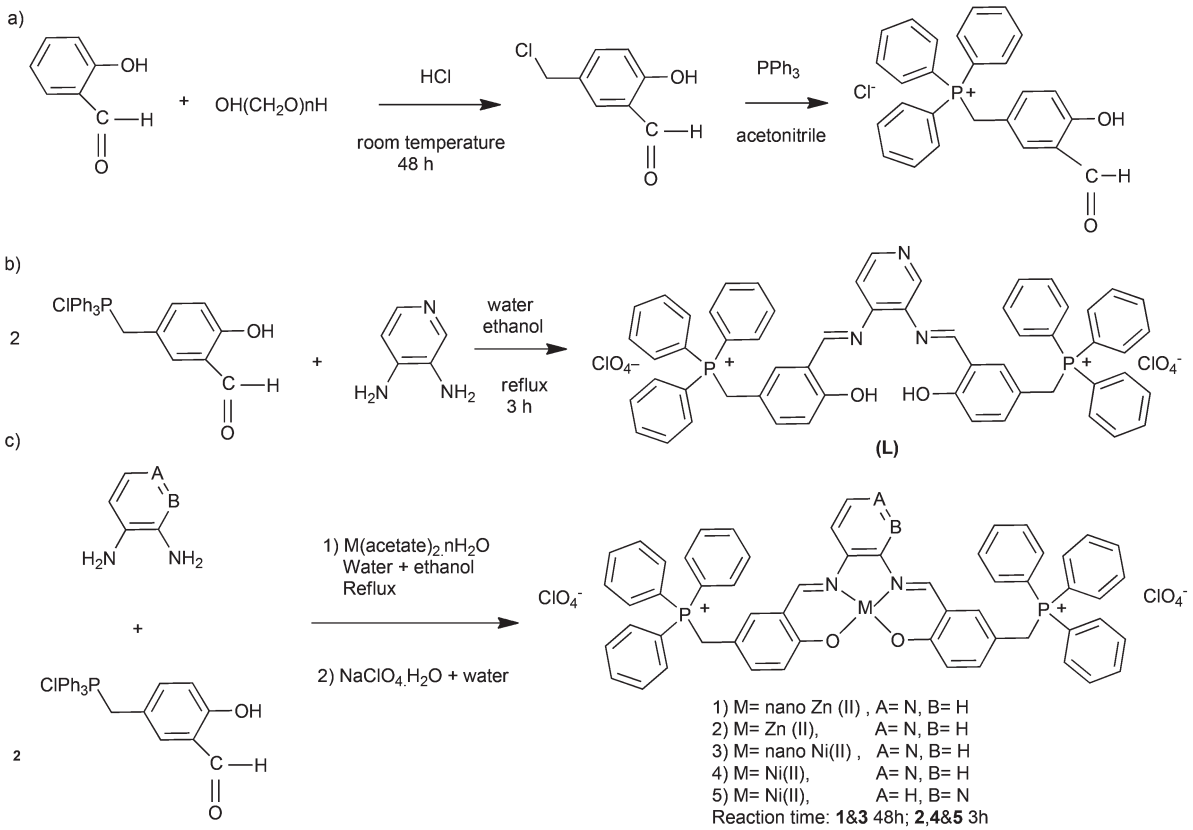

Scheme 1 Synthetic route for (a) (3-formyl-4-hydroxybenzyl)triphenylphosphonium chloride and (b) **L** (c) complexes **1–5**.

reference). ^{31}P NMR spectra in DMSO-d_6 were recorded using a Bruker Ultrashield 400 spectrometer (with 85% H_3PO_4 as the reference). UV-vis measurements were carried out using Perkin-Elmer (LAMBDA 2) UV-vis spectrophotometers. FT-IR spectra were recorded by using a Shimadzu FTIR 8300 infrared spectrophotometer. Elemental analysis was carried out by using a Thermo Fininngan-Flash 1200. Melting points of compounds were determined using a BUCHI 535. All experiments were carried out in triple distilled water at pH = 7.2, 1 mM Tris buffer and 5 mM NaCl.

Fluorescence spectra were recorded on a Perkin-Elmer (LS45) spectrofluorimeter equipped with a Lauda-ecoline-RE 104 thermostat at 37 °C. Transmission electron microscopy (TEM) images were obtained on a Zeiss EM10C transmission electron microscope using an Acc voltage of 80 kV. Field Emission Scanning Electron Microscopy (FE-SEM) images were obtained using a HITACHI S-4160 with a voltage of 20 kV. Electrochemistry studies were performed using an Auto lab 302N. An incubator and an ELISA reader (Biotek Instruments, Inc., USA) were used for anticancer studies.

Synthesis

(3-Formyl-4-hydroxybenzyl)triphenylphosphonium chloride. A mixture of salicylaldehyde (8.5 mL, 80 mmol), paraformaldehyde (1 mL, 50 mmol) and 50 mL of conc. HCl was stirred at room temperature for 48 h. The resulting dark red powder precipitate was collected by filtration, washed with 0.5% $NaHCO_3$ solution then with water until it became neutral, and dried in vacuum. The product (Scheme 1) was recrystallized from acetonitrile and petroleum ether. A mixture of 5-(chloromethyl) salicylaldehyde (10.2 g, 60 mmol) and triphenyl phosphine (15.7 g, 60 mmol) in 200 mL acetonitrile was refluxed for 4 h and cooled. The precipitated phosphonium salt was filtered off and washed with ether.

Yield: 85%. M.p. 250–251 °C. Color: white. Anal. calcd for $C_{26}H_{22}PO_2Cl$: C, 72.22; H, 5.12%. Found: C, 72.37; H, 5.24%. FT-IR (KBr, cm^{-1}): 3741.6 (ν_{OH}), 2869 (ν_{C-H}), 1674.1 ($\nu_{C=O}$). ^{1}H NMR (250 MHz, DMSO-d_6) δ (ppm): 11.18 (s, 1H, OH), 10.14 (s, 1H, CHO), 7.87 (dd, J = 10.1, 4.5 Hz, 3H, ArH), 7.69 (dq, J = 12.5, 7.6 Hz, 12H, ArH), 7.26–7.15 (m, 1H, ArH), 7.11–6.92 (m, 2H, ArH), 5.13 (d, J = 15.0 Hz, 2H, CH_2). ^{13}C NMR (63 MHz, DMSO-d_6) δ (ppm): 189.2 (CHO), 160.6, 137.9, 137.8, 135.0, 134.1, 134.0, 133.9, 133.8, 130.1, 130.1, 129.9, 129.8, 122.4, 122.4, 118.3, 118.0, 117.8, 116.9 (aromatic carbons), 34.2 (CH_2) (spectral data in Fig. S1–S3†).

[*N*,*N*′-Bis{5-[(triphenyl phosphonium chloride)-methyl] salicylidine}310-3,4-diaminopyridine](L). To a vigorously stirred solution of (3-formyl-4-hydroxybenzyl)triphenylphosphonium chloride (0.6 g, 1.25 mmol) in 50 mL water, an ethanolic solution (20 mL) of 3,4-diaminopyridine (0.07 g, 0.62 mmol) was added dropwise. The solution turned to light yellow and the mixture refluxed for 3 h. After that, $NaClO_4 \cdot H_2O$

(0.15 g, 1.25 mmol) dissolved in a minimum amount of water (5 mL) was added. The resulting yellow powder (Scheme 1) was collected by filtration, washed with cold ethanol and ether and dried in air.

[(5-CH_2PPh_3-3,4-salpyr)]$(ClO_4)_2$. Yield: 85%. M.p. >310 °C. Color: light yellow. Anal. calcd for $C_{57}H_{47}N_3Cl_2O_{10}P_2$: C, 62.08; H, 4.66; N, 3.81%. Found: C, 62.30; H, 4.81; N, 3.57%. FT-IR (KBr, cm^{-1}): 1650.9, ($\nu_{C=N}$), 1487.8 ($\nu_{C=C}$), 1087.8, 650.9 ($\nu_{ClO_4^-}$). UV-vis. (H_2O): λ_{max} (nm) = 387, 333. ^{1}HNMR (250 MHz, DMSO-d_6) δ (ppm): 11.12 (s, 2H, OH), 8.72 (s, 1H, HC═N), 8.53 (s, 1H, HC═N), 7.87 (d, J = 7.1 Hz, 8H, ArH), 7.68 (dd, J = 17.8, 4.4 Hz, 23H, ArH), 7.23–7.16 (m, 3H, ArH), 7.08–6.98 (m, 2H, ArH), 6.82 (d, J = 8.5 Hz, 3H, ArH), 5.06 (dd, J = 15.1, 3.1 Hz, 4H, CH_2P). ^{13}C NMR (63 MHz, DMSO-d_6) δ (ppm): 160.93, 160.88 (C═N), 138.0, 137.9, 135.0, 134.0, 133.9, 131.5, 130.4, 130.1, 129.9, 128.8, 122.4, 118.2, 118.0, 117.95, 116.9 (aromatic carbons), 34.24, 33.98 (CH_2). ^{31}P NMR (162 MHz, DMSO-d_6) δ (ppm): 22.58 (spectral data in Fig. S4–S8†).

Nano [*N*,*N*′-bis{5-[(triphenyl phosphonium chloride)-methyl] salicylidine}-3,4-diaminopyridine]zinc(II) perchlorate. [Zn(5-CH_2PPh_3-3,4-salpyr)]$(ClO_4)_2$ (1). The nano complex was synthesized by the slow addition of a solution of (3-formyl-4-hydroxybenzyl)triphenylphosphonium chloride (0.6 g, 1.25 mmol) in 50 mL water into a hot solution of Zn(acetate)$_2$·$2H_2O$ (0.14 g, 0.62 mmol) dissolved in water over 7 h and then a solution of 3,4-diaminopyridine (0.07 g, 0.62 mmol) in 20 mL ethanol was added into this mixture for 30 min. The solution turned to yellow and the mixture was refluxed for 40 h. After that, $NaClO_4$·H_2O (0.15 g, 1.25 mmol) dissolved in a minimum amount of water was added to the reaction mixture. The resulting yellow powder (Scheme 1) was collected by centrifugation, washed three times (3 × 2 mL) with ether and two times (2 × 1 mL) with cold ethanol and dried in vacuum.

A transmission electron microscopy (TEM) image showed nano-particles with sizes between 40–75 nm (Fig. 1a). [Zn(5-CH_2PPh_3-3,4-salpyr)]$(ClO_4)_2$. Yield: 91%. M.p. >310 °C. Color: yellow. Anal. calcd for $C_{57}H_{45}N_3Cl_2O_{10}ZnP_2$·$H_2O$: C, 59.62; H, 4.13; N, 3.66%. Found: C, 58.90; H, 4.00; N, 3.50%. FT-IR (KBr, cm^{-1}): 3440.8 (ν_{O-H}), 1620.1 ($\nu_{C=N}$), 1527.5 ($\nu_{C=C}$), 1110.9, 686.6 ($\nu_{ClO_4^-}$), 624.9 (ν_{M-O}), 501.5 (ν_{M-N}). UV-vis. (H_2O): λ_{max} (nm) = 386, 332. ^{1}HNMR (250 MHz, DMSO-d_6) δ (ppm): 10.31 (s, 1H, HC═N), 10.10 (s, 1H, HC═N), 9.12–8.39 (m, 1H, ArH), 7.88 (t, J = 7.3 Hz, 7H, ArH), 7.80–7.42 (m, 23H, ArH), 7.38 (d, J = 2.5 Hz, 1H, ArH), 7.27–7.06 (m, 2H, ArH), 6.99 (d, J = 4.7 Hz, 2H, ArH), 6.85–6.56 (m, 2H, ArH), 6.47 (d, J = 7.1 Hz, 1H, ArH), 5.03 (d, J = 14.7 Hz, 4H, CH_2). ^{13}C NMR (63 MHz, DMSO-d_6) δ (ppm): 162.1, 161.3 (C═N), 157.7, 149.7, 146.6, 144.7, 137.5, 135.0, 134.8, 134.0, 133.9, 130.2, 130.0, 129.6, 123.6, 123.2, 118.5, 117.7, 116.1, 113.7 (aromatic carbons), 34.6, 34.2 (CH_2). ^{31}P NMR (400 MHz, DMSO-d_6) δ (ppm): P_a (21.77), $P_{a'}$ (21.69) (spectral data in Fig. S9–S14†).

[*N*,*N*′-Bis{5-[(triphenyl phosphonium chloride)-methyl]salicylidine}-3,4-diaminopyridine]zinc(II) perchlorate. [Zn(5-CH_2PPh_3-3,4-salpyr)]$(ClO_4)_2$ (2). To a vigorously stirred solution of Zn(acetate)$_2$·$2H_2O$ (0.14 g, 0.62 mmol) in 25 mL water, a solution of (3-formyl-4-hydroxybenzyl)triphenylphosphonium chloride (0.6 g, 1.25 mmol) in 10 mL water and then an ethanolic solution (5 mL) of 3,4-diaminopyridine (0.07 g, 0.62 mmol) were added dropwise. The solution turned to dark yellow and the mixture refluxed for 3 h. After that, $NaClO_4$·H_2O (0.15 g, 1.25 mmol) dissolved in a minimum amount of water (5 mL) was added. The resulting yellow powder was collected by filtration, washed with cold ethanol and ether and dried in air. The complex was dissolved in CH_2Cl_2 (6 mL) and ethyl acetate (3 mL) and the resulting solution was allowed to evaporate slowly at room temperature. The solid product was filtered off and washed with ethyl acetate and ether.

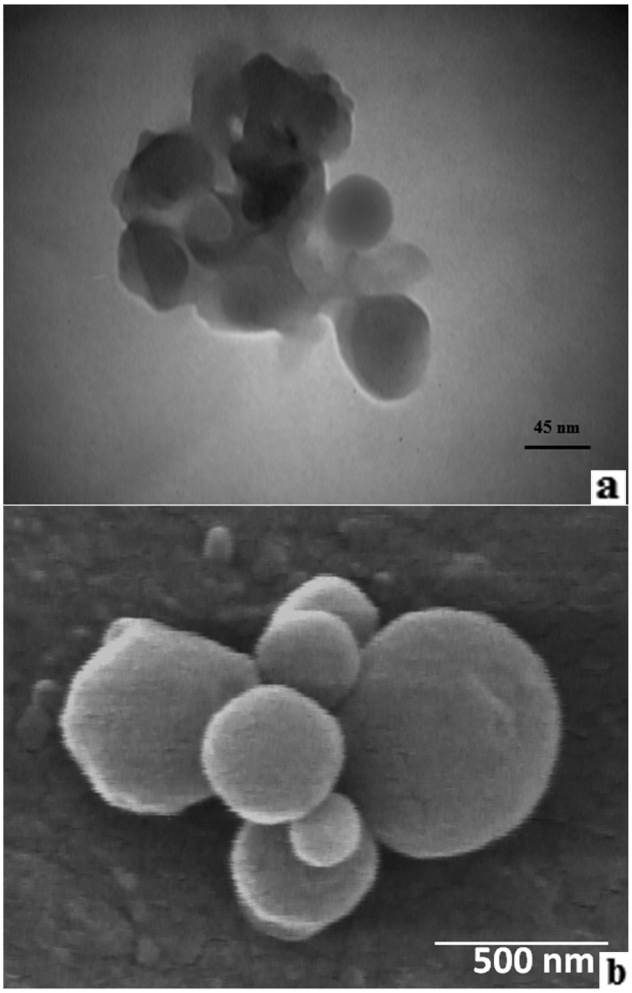

Fig. 1 (a) TEM and (b) FE-SEM images of nano-particles of Zn(5-CH_2PPh_3-3,4-salpyr)]$(ClO_4)_2$.

[Zn(5-CH_2PPh_3-3,4-salpyr)]$(ClO_4)_2$. Yield: 94%. M.p. >310 °C. Color: yellow. Anal. calcd for $C_{57}H_{45}N_3Cl_2O_{10}ZnP_2$·$H_2O$: C, 59.62; H, 4.13; N, 3.66%. Found: C, 59.40; H, 3.93; N, 3.50%. Spectral data (FT-IR, UV-vis, ^{1}H NMR, ^{13}C NMR and ^{31}P NMR) of complex (2) were the same as complex (1).

Nano [*N*,*N*′-bis{5-[(triphenyl phosphonium chloride)-methyl] salicylidine}-3,4-diaminopyridine]nickel(II) perchlorate. [Ni(5-CH_2PPh_3-3,4-salpyr)]$(ClO_4)_2$ (3). The nano complex was synthesized by slow addition of a solution of (3-formyl-4-

hydroxybenzyl)triphenylphosphonium chloride (0.6 g, 1.25 mmol) in 50 mL water into a hot solution of Ni(acetate)$_2$·4H$_2$O (0.15 g, 0.62 mmol) dissolved in water over 7 h and then a solution of 3,4-diaminopyridine (0.07 g, 0.62 mmol) in 20 mL ethanol was added to the mixture for 30 min. The solution turned to yellow and the mixture was refluxed for 48 h. After that, NaClO$_4$·H$_2$O (0.15 g, 1.25 mmol) was dissolved in a minimum amount of water added to the reaction mixture. The resulting red powder (Scheme 1) was collected by centrifugation, washed three times (3 × 2 mL) with ether and two times (2 × 1 mL) with cold ethanol and dried in vacuum.

A transmission electron microscopy (TEM) image showed nano-particles with sizes between 30–55 nm (Fig. 2a).

[Ni(5-CH$_2$PPh$_3$-3,4-salpyr)](ClO$_4$)$_2$. Yield: 92%. M.p. >310 °C. Color: red. Anal. calcd for $C_{57}H_{45}N_3Cl_2O_{11}NiP_2$: C, 59.97; H, 4.15; N, 3.68%. Found: C, 59.70; H, 3.95; N, 3.40%. FT-IR (KBr, cm^{-1}): 1620.1 ($\nu_{C=N}$), 1527.5 ($\nu_{C=C}$), 1095.5, 694.9 ($\nu_{ClO_4^-}$), 624.9 (ν_{M-O}), 501.5 (ν_{M-N}). UV-vis (H$_2$O): λ_{max} (nm) = 476, 375. ^{1}H NMR (250 MHz, DMSO-d$_6$) δ (ppm): 9.45 (s, 1H, HC═N), 9.30 (s, 1H, HC═N), 8.50 (t, J = 5.1 Hz, 1H, ArH), 8.05 (t, J = 5.5 Hz, 1H, ArH), 7.98–7.82 (m, 7H, ArH), 7.80–7.57 (m, 24H, ArH), 7.31 (s, 2H, ArH), 6.83 (dd, J = 8.4, 4.1 Hz, 2H, ArH), 6.64 (dd, J = 9.5, 3.9 Hz, 2H, ArH), 5.06 (d, J = 14.5 Hz, 4H, CH$_2$). ^{13}C NMR (63 MHz, DMSO-d$_6$) δ (ppm): 162.4, 161.6 (C═N), 155.7, 150.5, 146.2, 142.2, 140.3, 139.5, 138.7, 135.0, 134.0, 133.9, 130.2, 130.0, 126.8, 126.0, 122.4, 122.0, 118.5, 117.3, 10.4.6 (aromatic carbons), 34.9, 34.1 (CH$_2$). ^{31}P NMR (400 MHz, DMSO-d$_6$) δ (ppm): P$_a$ (21.90), P$_{a'}$ (21.75) (spectral data in Fig. S15–S20†).

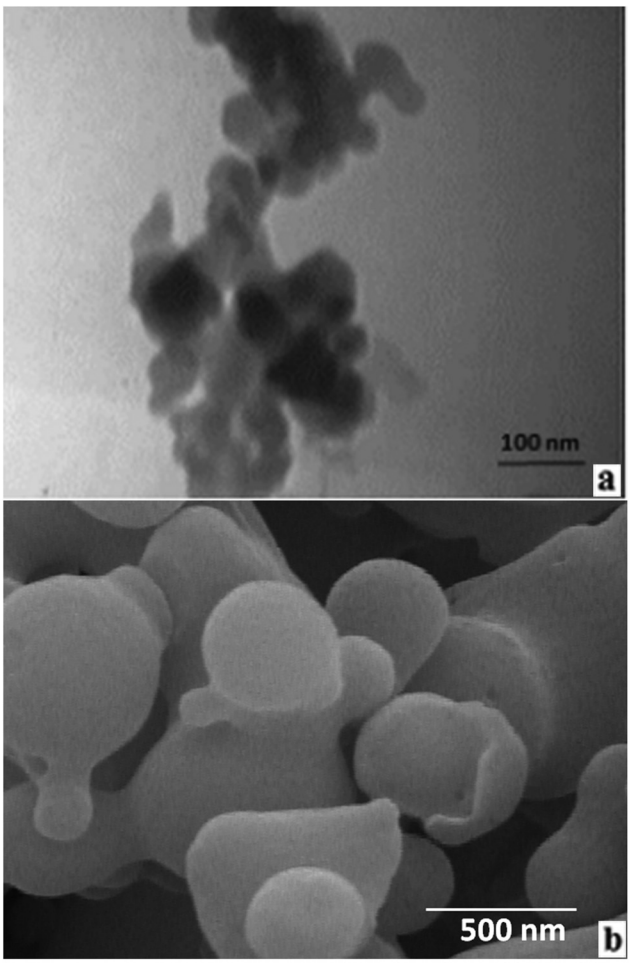

Fig. 2 (a) TEM and (b) FE-SEM images of nano-particles of Ni(5-CH$_2$PPh$_3$-3,4-salpyr)](ClO$_4$)$_2$.

[*N*,*N*′-Bis{5-[(triphenyl phosphonium chloride)-methyl]salicylidine}-3,4-diaminopyridine]nickel(II) perchlorate. [Ni(5-CH$_2$PPh$_3$-3,4-salpyr)](ClO$_4$)$_2$ (4). To a vigorously stirred solution of Ni(acetate)$_2$·4H$_2$O (0.15 g, 0.62 mmol) in 25 mL water, a solution of (3-formyl-4-hydroxybenzyl)triphenylphosphonium chloride (0.6 g, 1.25 mmol in 10 mL water) and then an ethanolic solution (5 mL) of 3,4-diaminopyridine (0.07 g, 0.62 mmol) were added dropwise. The solution turned to dark red and the mixture refluxed for 3 h. After that, NaClO$_4$·H$_2$O (0.15 g, 1.25 mmol) dissolved in a minimum amount of water (5 mL) was added. The resulting red powder was collected by filtration, washed with cold ethanol and ether and dried in air. The complex was dissolved in CH$_2$Cl$_2$ (6 mL) and ethyl acetate (3 mL) and the resulting solution was allowed to evaporate slowly at room temperature. The solid product was filtered off and washed with ethyl acetate and ether.

[Ni(5-CH$_2$PPh$_3$-3,4-salpyr)](ClO$_4$)$_2$. Yield: 90%. M.p. >310 °C. Color: red. Anal. calcd for $C_{57}H_{45}N_3Cl_2O_{11}NiP_2$: C, 59.97; H, 4.15; N, 3.68%. Found: C, 59.62; H, 3.95; N, 3.49%. Spectral data (FT-IR, UV-vis, ^{1}H NMR, ^{13}C NMR and ^{31}P NMR) of complex (**4**) were the same as complex (**3**).

[*N*,*N*′-Bis{5-[(triphenyl phosphonium chloride)-methyl]salicylidine}-2,3-diaminopyridine]nickel(II) perchlorate. [Ni(5-CH$_2$PPh$_3$-2,3-salpyr)](ClO$_4$)$_2$ (5). To a vigorously stirred solution of Ni(acetate)$_2$·4H$_2$O (0.15 g, 0.62 mmol) in 25 mL water, a solution of (3-formyl-4-hydroxybenzyl)triphenylphosphonium chloride (0.6 g, 1.25 mmol) in 10 mL water and then an ethanolic solution (5 mL) of 2,3-diaminopyridine (0.07 g, 0.62 mmol) was added dropwise. The solution turned to dark red and the mixture refluxed for 3 h. After that, NaClO$_4$·H$_2$O (0.15 g, 1.25 mmol) dissolved in a minimum amount of water (5 mL) was added. The resulting red powder was collected by filtration, washed with cold ethanol and ether and dried in air. The complex was dissolved in CH$_2$Cl$_2$ (6 mL) and ethyl acetate (3 mL) was added and the resulting solution was allowed to evaporate slowly at room temperature. The solid product was filtered off and washed with ethyl acetate and ether.

[Ni(5-CH$_2$PPh$_3$-2,3-salpyr)](ClO$_4$)$_2$. Yield: 91%. M.p. >310 °C. Color: red. Anal. calcd for $C_{57}H_{45}N_3Cl_2O_{11}NiP_2$: C, 59.97; H, 4.15; N, 3.68%. Found: C, 60.09; H, 3.88; N, 4.00%. FT-IR (KBr, cm^{-1}): 1620.1 ($\nu_{C=N}$), 1527.5 ($\nu_{C=C}$), 1095.5, 694.9 ($\nu_{ClO_4^-}$), 624.9 (ν_{M-O}), 501.5 (ν_{M-N}). UV-vis. (H$_2$O): λ_{max} (nm) = 472, 375. ^{1}H NMR (250 MHz, DMSO-d$_6$) δ (ppm): 9.28 (s, 1H, HC═N), 9.14 (s, 1H, HC═N), 8.03 (s, 1H, ArH), 7.98–7.81 (m, 7H, ArH), 7.80–7.51 (m, 24H, ArH), 7.44–7.14 (m, 3H, ArH), 7.04 (d, J = 7.3 Hz, 1H, ArH), 6.83 (d, J = 7.3 Hz, 2H, ArH), 6.65–6.47 (m, 1H, ArH), 5.06 (d, J = 13.7 Hz, 4H, CH$_2$).

^{13}C NMR (63 MHz, DMSO-d_6) δ (ppm): 162.7, 161.5 (C═N), 155.2, 150.2, 146.3, 142.5, 140.7, 139.0, 138.0, 135.7, 134.2, 133.0, 130.8, 130.0, 126.4, 126.0, 122.5, 122.3, 118.0, 117.0, 10.4.5 (aromatic carbons), 34.7, 34.5 (CH_2). ^{31}P NMR (400 MHz, DMSO-d_6) δ (ppm): Pa, Pa′ (22.59) (Spectral data in Fig. S21–S25†).

***CAUTION**! The perchlorate salts could be potentially explosive. Therefore, only small quantities of the sample were handled to avoid any possible explosion.*

Solubility and stability

The complexes were soluble in water, dimethyl formamide (DMF) and dimethyl sulfoxide (DMSO). The complexes were stable in the solid phase at ambient temperature in the light. The solutions were stable on keeping for a long period in light.

DNA binding experiments

Concentrated stock solutions of metal complexes were prepared by dissolving them in 1 mM Tris HCl/5 mM NaCl buffer at pH 7.2 and diluting suitably with the corresponding buffer to the required concentrations for all the experiments. The DNA concentration was measured from its absorption intensity at 260 nm using a molar absorption coefficient value of 6600 $dm^3\ mol^{-1}\ cm^{-1}$.[62]

The absorption spectra were recorded on a Perkin-Elmer lambda 2 UV-Vis spectrophotometer. A solution of DNA in the buffer gave a ratio 1.98, of UV absorbance at 260 and 280 nm, A_{260}/A_{280}, indicating that the DNA was sufficiently free from protein. In these experiments, 3 mL of the complex solutions ([Ni] = 20 μM, [Zn] = 90 μM) were poured into the cell. Absorbance spectra were recorded after each successive addition (10 μL) of DNA solution and equilibration (*ca*. 4 min) at 310 K. The binding of metal complexes to DNA has been studied through the changes in absorbances and shifts in wavelength. In order to obtain a more quantitative determination of the interaction strength, the intrinsic-binding constant, K_b, was determined using spectroscopic titration data at various wavelengths where the difference in absorption was the maximum after equilibrium.

An Ostwald viscometer was used for viscosity measurements. The temperature was constant at 25 ± 0.5 °C by using a temperature bath.

The concentration of DNA was 10 μM, and flow time was measured with a digital stopwatch. The mean values were used to evaluate the viscosity η of the samples. The values for relative specific viscosity $(\eta/\eta_o)^{1/3}$, where η_o and η are the specific viscosity contributions of DNA in the absence (η_o) and in the presence of the complex (η), were plotted against r_i (r_i = [complex]/[DNA] = 0, 0.05, 0.10, 0.15, 0.20, 0.25).

Cyclic voltammetry was carried out using a CH Instruments electrochemical analyser. All voltammetric experiments were performed in a single compartmental cell of volume 10–15 mL containing a three-electrode system comprising a Pt working electrode, a reference electrode (Ag/Ag^+ in TBAP/acetonitrile solution), and a Pt auxiliary electrode. The measurements of CV for H_2O–DMSO solution containing Schiff base complexes (1.0×10^{-3} M) were carried out in the potential range from −1.0 V to 1.5 V. Electrochemistry of these newly synthesized Schiff base metals was studied by cyclic voltammetry at a scan rate of 0.10 V s^{-1} in H_2O–DMSO solution.

Circular dichroic spectra of DNA were obtained by using a JASCO J-716 spectropolarimeter equipped with a Peltier temperature control device. All experiments were done using a 1 or 0.2 cm path quartz cell. Each CD spectrum was collected after averaging over at least 2 accumulations using a scan speed of 100 nm min^{-1} and a 1 s response time. Machine plus cuvette baselines were subtracted and the resultant spectrum zeroed outside the absorption bands.

Emission intensity measurements were carried out using a Perkin-Elmer (LS45) spectrofluorimeter with 10 nm excitation and 10 nm emission slit widths. The excitation wavelength was fixed and the emission range was adjusted before measurements. The samples were placed in quartz cuvettes of 1 cm optical path. In these experiments, 3 mL of the complex solution (5 μM) were poured into the cell. Emission spectra were recorded after each addition (10 μL) of DNA solution (10^3 μM) into the same buffer at 310 K. The observed fluorescence intensities were also corrected for dilution. The reaction time has been studied and the results showed that 4 min was enough for stabilization. So the change in fluorescence emission intensity was measured within 4 min after each addition.

DNA cleavage and ethidium bromide competitive studies

Gel electrophoresis experiments were performed using 500 ng supercoiled pBlu2KSM DNA in 10 mM Tris-HCl buffer pH 7.2 (in 1% DMSO) with the final concentrations of 10–100 μM metal complexes in a total volume of 10 μl. The samples were then incubated for 1 h at 37 °C, followed by electrophoresis on 1% agarose gel in TAE buffer containing 1.0 μg ml^{-1} ethidium bromide at 60 V for 1 h and finally, photographed under UV light. The efficiency of the cleavage activity of the complexes was determined by the ability of the complex to cause single or double strand breaks in DNA and form a linear form (LF) or nicked circular (NC) DNA compared to its supercoiled (SC) ones.

Anticancer activity studies

Cell viability tests were performed against two cell lines including human hepatoma (HepG2) and cervical cancer cell (HeLa) with MTT assay as described previously.[63] The stock solutions of the metal complexes were prepared in DMSO ranging from 0.1 to 1% with regard to the fact that DMSO was found to be non-toxic to the cells until 1% concentration. Then the cells were treated with series of different concentrations of DMSO dissolved ligand ranging from 1–100 μg ml^{-1} 24 h after seeding of 5×10^3 cells per well in 200 μl of fresh culture medium and DMSO was used as the negative control. After 24 and 48 h, 20 μl of MTT solution (5 mg ml^{-1} in PBS buffer) was added to each well and the plates were wrapped with aluminium foil and incubated for 4 h at 37 °C. The purple formazan product formed was dissolved by the addition of 100 μl of 100% DMSO to each well. The absorbance was monitored at 570 nm

(measurement) and 630 nm (reference) using a 96 well plate reader (Biotek Instruments, Inc., USA).[64] Data were collected for three replicates each and were used to calculate the mean. The percentage of inhibition was calculated from these data using the formula:

$$\frac{\text{Mean OD of untreated cells (control)} - \text{Mean OD of treated cells}}{\text{Mean OD of untreated cells (control)}} \times 100$$

Theoretical calculations

Geometry optimization was performed with the hybrid density functional theory method by Becke's hybrid three-parameter exchange functional and the nonlocal correlation functional of Lee, Yang, and Parr (B3LYP). The Hay and Wadt basis set LANL2DZ was used for the metal centers while for the rest of the atoms the 6-311G* standard basis set was employed.[65] All structures were fully optimized in the gas phase with default convergence criteria. The Gaussian 03 software package was used for all computations.[66]

Molecular docking

The molecular geometry of **L**, complexes **1**, **3** and **5** were subjected to energy minimization by DFT calculations by the B3LYP method using the LANL2DZ basis set for the central atoms and 6-311G* for all the non-metal atoms for ground state geometry optimization.

The crystal structures of 3US0 (pdb code d(AAACATGTTTA-TAAACATGTTT) was selected from the Protein Data Bank (http://www.pdb.org),[67] the protein molecules were removed from this structure before performing docking calculations which had been equilibrated at a nuclei-like condition[68] and used as the receptor.

Then, the optimized ligands were imported to the Molegro Virtual Docker (MVD)[69] to carry out the docking simulations. This software generates the best DNA–ligand configurations according to several scoring criteria such as Moldock and Rerank scores.

In MVD the units are arbitrary, but an ideal hydrogen bond contributes to the overall energy.[70] We have selected the score as the Moldock score [GRID], with a GRID resolution of 0.3 Å. The algorithm selected for docking was Moldock along with a number of runs as 20.[71] For each docking calculation, 10 different poses were requested. All other parameters were kept at their default values. Parameter settings, pose generation and simplex evolution were selected as default settings. After docking energy minimization is an essential parameter along with optimized hydrogen bonding.

Results and discussion

Syntheses and spectral properties of complexes

The complexes $[M(5\text{-}CH_2PPh_3\text{-}3,4\text{-salpyr})](ClO_4)_2$ (M = Zn (**1**, **2**) Ni (**3**, **4**) show that the complexes **1** and **3** were synthesized with nano size) and $[Ni(5\text{-}CH_2PPh_3\text{-}2,3\text{-salpyr})](ClO_4)_2$ (**5**) were isolated using the procedure reported (Scheme 1).

All the complexes were characterized by elemental analysis, FT-IR, ^{1}H NMR, ^{13}C NMR,^{31}P NMR, UV-vis spectroscopy and the morphology of the nano complexes were determined using FE-SEM and TEM. ^{1}H NMR spectral data of the zinc and nickel complexes are given in the Experimental section. The ^{1}H NMR spectra of **L** and complexes **1–5** showed a complex overlap of signals in the δ 6.50–7.90 ppm range corresponding to aromatic protons of the ligand and coordinated triphenylphosphine.[72] A doublet corresponding to the azomethine group was observed at the ~8.50–9.50 ppm range.[73] In the spectra of the ligand, the singlet appearing at δ 11.09 ppm is assigned to the OH group. However, in the spectra of the complexes there was no resonance attributable to OH, indicating the coordination of ligand in the anionic form upon deprotonation. A doublet corresponding to the CH_2P appeared at δ 5.00–5.10 ppm in the compounds.

In the ^{13}C NMR spectra, the azomethine carbon resonance is observed at 160.0–163.0 ppm. In all compounds, aromatic carbon atoms were observed around 103.0–157.0 ppm. Three signals corresponding to the presence of triphenylphosphine observed at 138.0–116.9 ppm (**L**), 157.7–113.7 ppm (complexes **1** and **2**) and 155.7–104.6 ppm (complexes **3–5**) are in the range of the reported values.[74] The CH_2 carbon resonance is observed at 30.0–34.0 ppm.

In order to confirm the presence of triphenylphosphine, ^{31}P NMR spectra were recorded. Two peaks observed at 20.0–23.0 ppm suggested the presence of two non-equivalent triphenylphosphines.

Electronic spectral data for the complexes in H_2O are given in the Experimental section. These complexes show intensive absorption bands at 220–380 nm, which are attributed to the $\pi \rightarrow \pi^*$ transition in aromatic rings or azomethine groups and the $n \rightarrow \pi^*$ transition in the pyridine ring.

The FT-IR spectrum of aldehyde exhibited a broad medium intensity band at 3741 cm^{-1} due to the O–H. The medium–weak band at 1674 cm^{-1} was assigned to the CHO bond. The structure of the Schiff base complexes was indicated by the presence of strong imine (C=N) bands at 1620 cm^{-1}. Two peaks around 1110 and 700 cm^{-1} were related to the ClO_4^- group. The vibration band for the complexes around 3440 cm^{-1} was attributed to the presence of lattice and coordinated water.[75] The medium-weak bands at 2990 and 3050 cm^{-1} are observed for the aromatic (C–H) stretching bands. The phenolic (C–O) stretching bands, because of the participation of oxygen in the C–O–M bond, are observed in the region of 1200–1220 cm^{-1}. The ring skeletal vibrations (C=C) were consistent in the region of 1440–1550 in all complexes.[76] In the lower frequency region, the medium–weak bands observed at 551–563 and 435–458 cm^{-1} have been assigned respectively to the (M–N) and (M–O) vibrations.[77,78]

The SEM and TEM images of nano complexes (**1**, **3**) are shown in Fig. 1 and 2. The TEM image of complex **1** shows

that the average size of the nano Zn(II) complex was around 40–75 nm (Fig. 1a). The morphology and size of nano complex **1** were studied by FE-SEM and it seems that the particles are semispherical and confirmed the result of TEM (Fig. 1b).

The average size of the nano Ni(II) complex **3** was detected by TEM as around 30–55 nm (Fig. 2a). The FE-SEM of nano complex **3** shows semispherical morphology for nano Ni(II) complex **3** and the average size was shown to be the same as in the TEM study (Fig. 2b).

DNA binding studies

Absorption spectral studies. Electronic absorption spectroscopy is one of the most common methods to explore the interaction of compounds with DNA. The change in absorbance and shift in wavelength upon addition of DNA solution in a fixed concentration of metal complexes gives important information on the type of interaction. A compound binding to DNA through intercalation usually results in hypochromism with or without a red or blue shift, because of the intercalative mode concerning a strong stacking interaction between the planar aromatic chromophore and the base pairs of DNA.[79,80]

The range of hypochromism is usually consistent with the strength of the intercalative binding interaction.[81] The hypochromicity is specific to the interaction between the electronic states of the compound chromophores and those of the DNA bases, meanwhile the red shift is concomitant with the decrease in the energy gap between the highest occupied and lowest unoccupied molecular orbitals (HOMO and LUMO) after binding of the complex to DNA.[82,83] The absorption spectra of Ni(II) complexes with DNA are shown in Fig. 3. Upon increasing the concentration of DNA in the solution of the Ni complexes, the bands at 375 nm showed hypochromism and a red-shift, indicating that the interaction with DNA results in the direct formation of a new complex with double-helical DNA resulting in stabilization of the DNA duplex, while Zn(II) complexes exhibit both hypochromism and hyperchromism for the 386 nm and 330 nm bands, respectively without shifts in the band position. The overall spectral changes with hypochromicity and isosbestic point induced by binding planar polyaromatic molecules to DNA are suggestive of strong interactions. Also the hyperchromic effect ascends mainly because of the presence of charged cations which bind to DNA *via* electrostatic attraction to the phosphate group of the DNA backbone and hence causing a contraction and overall damage to the secondary structure of DNA.[84] The hyperchromic effect may also be ascribed to external contact (electrostatic binding)[85] or to partial untwisting of the helix structure of DNA, exposing more bases of the DNA.[86] These spectroscopic characteristics suggest that the complexes had some interaction with DNA. The basic binding constant K_b is a useful tool to define the magnitude of the binding strength of compounds with DNA. For Ni complexes the intrinsic binding constant of the complex, K_b, was determined by using the nonlinear least-squares fitting analyses.[87,88]

$$\frac{\varepsilon_a - \varepsilon_f}{\varepsilon_b - \varepsilon_f} = \frac{b - \left(b^2 - \frac{2K_b^2 C_t\,[\mathrm{DNA}]}{s}\right)^{1/2}}{2K_b C_t} \quad (1)$$

$$b = 1 + k_b C_t + \frac{K_b[\mathrm{DNA}]}{2s} \quad (2)$$

where ε_a is the extinction coefficient observed for the absorption band at a given DNA concentration, ε_f is the extinction coefficient of the complex free in solution, and ε_b is the extinction coefficient of the complex when fully bound to DNA. The intrinsic binding constants K_b of the complexes **3–5** were in the 1.70×10^6–1.38×10^7 range. These values are comparable to that observed for classical intercalators whose K_b values are in the order of 10^7 M^{-1}.[89] The intrinsic binding constants of **L** and complexes **1**, **2** with DNA were obtained by monitoring the changes in the absorbance of the LMCT band of the complexes with the increasing concentration of DNA using functional eqn (3):[90]

$$[\mathrm{DNA}]/(\varepsilon_a - \varepsilon_f) = [\mathrm{DNA}]/(\varepsilon_b - \varepsilon_f) + 1/k_b(\varepsilon_b - \varepsilon_f) \quad (3)$$

where [DNA] is the concentration of DNA in base pairs, ε_a, ε_f and ε_b correspond to A_{obs}/[complex], the extinction coefficient of the free complex, and the extinction coefficient of the complex in the fully bound form, respectively. K_b was obtained from the ratio of the slope to intercept by using the plot of $[\mathrm{DNA}]/(\varepsilon_a - \varepsilon_f)$ *vs.* [DNA] (Table 1).

The intrinsic binding constants K_b of the Zn(II) complexes were in the range 3.3×10^3–2.2×10^3 M^{-1}. However, the observed binding constant is smaller than the classical intercalators and metallointercalators where the binding constant was reported to be in the order of 10^7 M^{-1},[91] but they are comparable to the observed value for some complexes like $[Co(phen)_3]^{3+}$ (1.6×10^4 M^{-1});[92] $[Ru(phen)_3]^{2+}$ (0.55×10^4 M^{-1});[93] $[Zn(flmq)_2(bipy)]$ (4.71×10^4 M^{-1});[94] $[Zn(flmq)_2(H_2O)_2]$ (7.93×10^4 M^{-1});[93] $[Zn(erx)_2(bipy)]$ ($K_b = 2.61 \times 10^4$ M^{-1});[95] $[NiL^1(NH_3)]$ ($K_b = 2.3 \times 10^4$ M^{-1});[96] $[NiL^5(H_2O)]\cdot H_2O$ ($K_b = 1.99 \times 10^4$ M^{-1});[96] tricationic Co(III) complexes with an asymmetric ligand, $[Co(phen)_2(pdta)]^{3+}$ ($K_b = 2.8 \times 10^4$);[97] $[Co(bpy)_2(CNOIP)]^{3+}$ ($K_b = 5 \times 10^4$ M^{-1}).[98]

The achieved values indicate that the Zn(II) complexes are moderately bound to FS-DNA[89] and electrostatic interactions cannot be ruled out.

From the results obtained, it has been found that the complexes strongly bound with DNA relative to the ligand and Ni(II) complexes are better relative to Zn(II) complexes. Furthermore the size of particles influences the interaction. The order of binding affinity is **3** > **4** > **5** > **1** > **2** > **L**.

The effective nuclear charge for the Zn atom is more than the Ni atom so it seems that the electrostatic interaction with DNA is more likely for the Zn complexes; on the other hand the square planer structure for Ni (d^8 complexes) is more responsible for the strong intercalative interaction with respect to the Zn complexes (d^{10}) with the tetrahedral structure which correlates well with their strong DNA binding affinity.

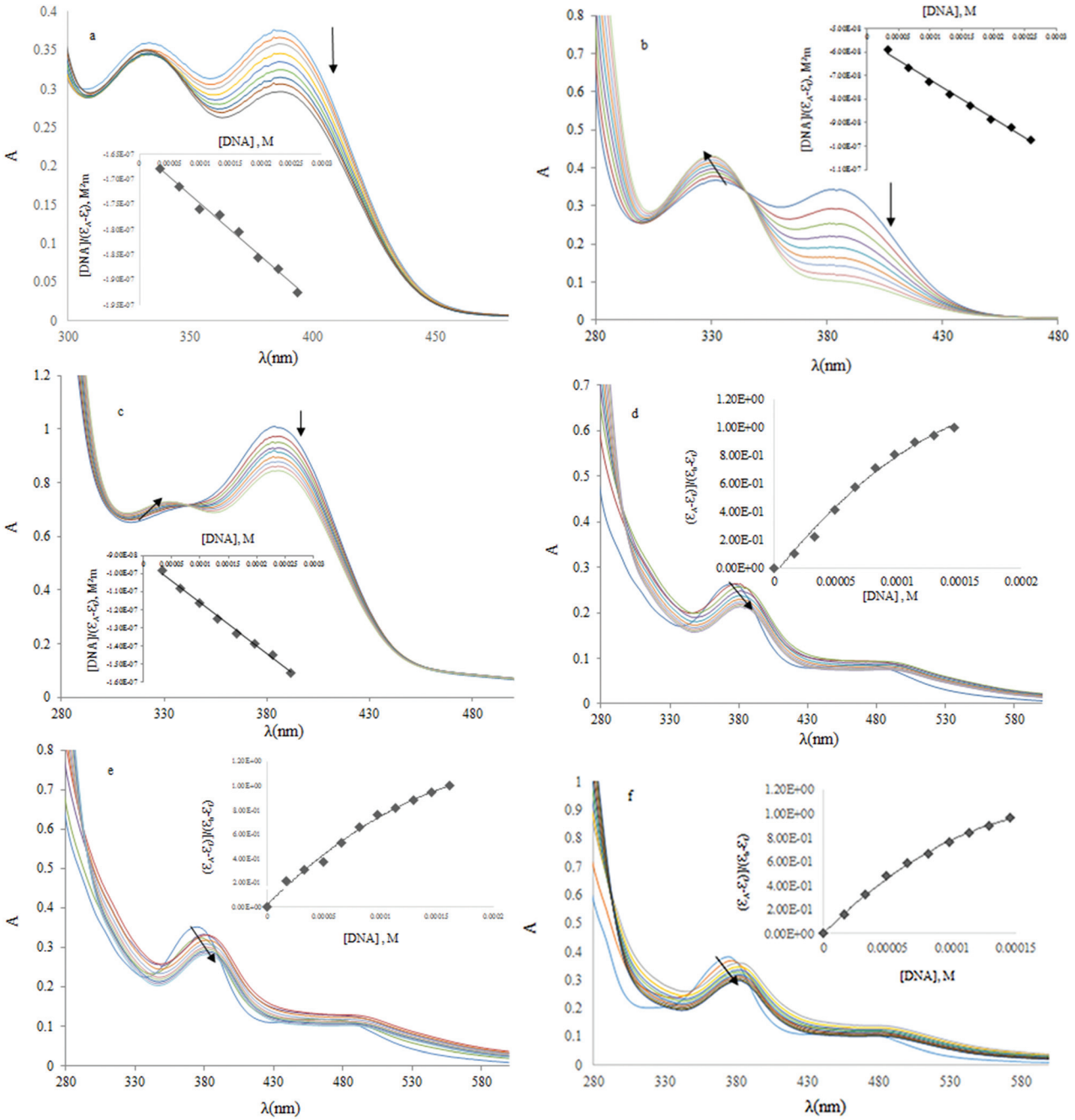

Fig. 3 Absorption spectra of (a) **L** (50 μM), (b, c) complexes **1**, **2** (90 μM) and (d–f) complexes **3–5** (20 μM) in 1 mM Tris HCl buffer at pH 7.2, in the absence and presence of increasing amounts of DNA (0–260 μM in (a–c) and 0–146 μM in (d–f). Insets: plot of [DNA]/($\varepsilon_a - \varepsilon_f$) *vs.* [DNA] for **L**, **1**, **2** and the least squares fit of ($\varepsilon_a - \varepsilon_f$)/($\varepsilon_b - \varepsilon_f$) *vs.*[DNA] using the MvH-equation for **3–5**.

The results derived from the UV titration experiments propose that all complexes can bind to DNA although the exact mode of binding cannot be only suggested by UV spectroscopic titration studies.[99] Nonetheless, the existence of hypochromism for the complexes could be considered as the first evidence that the binding of the complexes involving intercalation between the base pairs of DNA cannot be ruled out. The different behaviors between the complexes may be attributed to the z^* effect and geometry. The complexes exhibited more hypochromicity than the ligand, signifying that the binding strength of the complexes is much stronger than that of the free ligands. Intercalation is the most possible binding mode between Ni(II) complexes and DNA because of the more planar aromatic structure of these complexes, but the intercalative ability of Zn(II) complexes to DNA appears weak and suggests the involvement of **L** and **1**, **2** in DNA groove binding.

Table 1 Absorption spectral properties of compounds bound to DNA, concentrations of solution L and complexes at pH 7.2 in buffer solutions are 50 μM (L), 90 μM (1, 2), 20 μM (3–5)

Compound	λ (nm)	Change in absorbance	Red shift (nm)	$K_b(M^{-1})$	s_{opt}
L	387	Hypochromism	0	0.25×10^3	
1	386	Hypochromism	0	3.33×10^3	
2	386	Hypochromism	0	2.22×10^3	
3	375	Hypochromism	8	13.84×10^6	1.0
4	375	Hypochromism	7	9.99×10^6	1.3
5	375	Hypochromism	6	1.70×10^6	1.1

Viscosity measurements

Viscosity measurement is often considered as an effective mode to determine the binding mode between small molecules and DNA. Intercalating agents are expected to lengthen the double helix to accommodate the ligands in between the bases, leading to an increase in the viscosity of DNA.[100] However, for the electrostatic or groove binding, there is a slight effect on the viscosity of DNA.[101] The values of relative specific viscosity (η/η_o), where η and η_o are the specific viscosities of DNA in the presence and absence of the complex, are plotted against r (= [Complex]/[DNA]) (Fig. 4). When small planar aromatic molecules intercalate between the neighboring base pairs of DNA, the double helix loosens to accommodate the intercalation, which increases the length of the DNA helix. Since the viscosity of DNA solution is very sensitive to the changes of DNA length, the increased viscosity of DNA solution can be associated with the specific intercalation binding mode. The results reveal that the presence of the three Ni(II) complexes has a significant effect on the viscosity of FS-DNA solution. The increased degree of viscosity, which may depend on its affinity to DNA, follows the order of **3** > **4** > **5**, which parallels the hypochromism and DNA binding affinities. As shown in Fig. 4, the viscosities of DNA in the Tris-HCl buffer solution almost do not change with the increasing concentration of Zn(II) complexes, indicating that the binding mode of DNA with **1**, **2** may be the groove binding.

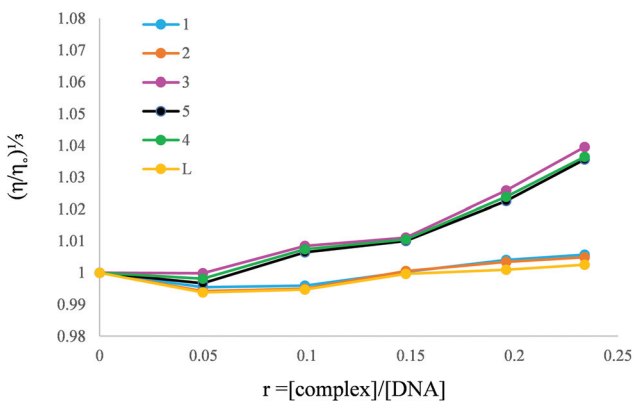

Fig. 4 Effects of increasing amounts of L and complexes (**1**–**5**) (0–2.34 μM) on the viscosity of DNA (10 μM) in 1 mM Tris-HCl buffer (r = 0.0–0.25) at 25 °C.

Circular dichroism spectroscopy

Circular dichroic spectroscopy is a useful method for monitoring changes in the DNA structure in solution and provides information about binding interactions with DNA. The CD spectrum of free DNA is of the typical B-form, with a positive Cotton effect near 275 nm due to base stacking and a negative Cotton effect near 245 nm due to right-handed helicity[102] and these bands are quite sensitive to the mode of DNA interactions with small molecules. Thus simple groove binding and electrostatic interaction of small molecules display small or no perturbation on the base-stacking and helicity bands, while the classical intercalation increases the base stacking and stabilizes helicity, and so enhances the intensity of the positive band.[103]

Fig. 5 depicts the CD spectra of DNA with increasing concentrations of metal complexes. The addition of complex **1** to the solution of DNA induced a decrease in intensity for the negative band at ~245 nm and the positive band at ~275 nm with a small blue shift of about 4 nm (Fig. 5a), suggesting that the stacking mode and the orientation of base pairs in DNA were disturbed. The same result for complex **2** was observed (Fig. S26a†).

The phenomenon for complex **3** was similar to that for complex **1** at ~275 nm bands, while a much larger decrease in intensity for the positive band at ~275 nm and a new small positive band at ~244 nm were observed as shown in Fig. 5b. Since such a band and the shift of the main positive band toward shorter waves were characteristic of Z-DNA, it may mean that the DNA strands were locally converted into Z-DNA forms.[104] The same result for complex **4** was observed but with a lower decrease in intensity (Fig. S26b†). For complex **5** (Fig. 5c), there was a decrease in intensity for the negative band at ~245 nm and for the positive band at ~275 nm without a shift in the band positions. This showed that the DNA would interact with these complexes and might be distorted into other structures.[105]

The decrease of the intensity of the positive band (275 nm) was likely to be because of a transition from the extended nucleic acid right-handed double helix to a more compact form,[106] so the conformation of DNA had partly changed due to the binding interaction between these complexes and DNA.

Electrochemical studies

Cyclic voltammetry has demonstrated to be a very sensitive analytical method to determine changes in the redox behaviour of metallic species in the presence of biologically important molecules.[107,108] The electrochemical examinations of metal–DNA interactions can provide a valuable complement to spectroscopic methods, *e.g.*, for non-absorbing types, and yield information about interactions with both the reduced and oxidized forms of the metal.[109] Cyclic voltammetry of complexes (**1**–**4**) in H_2O/DMSO showed oxidation waves in the sweep range from −1 V to +1.5 V (Fig. 6). In the absence of DNA,

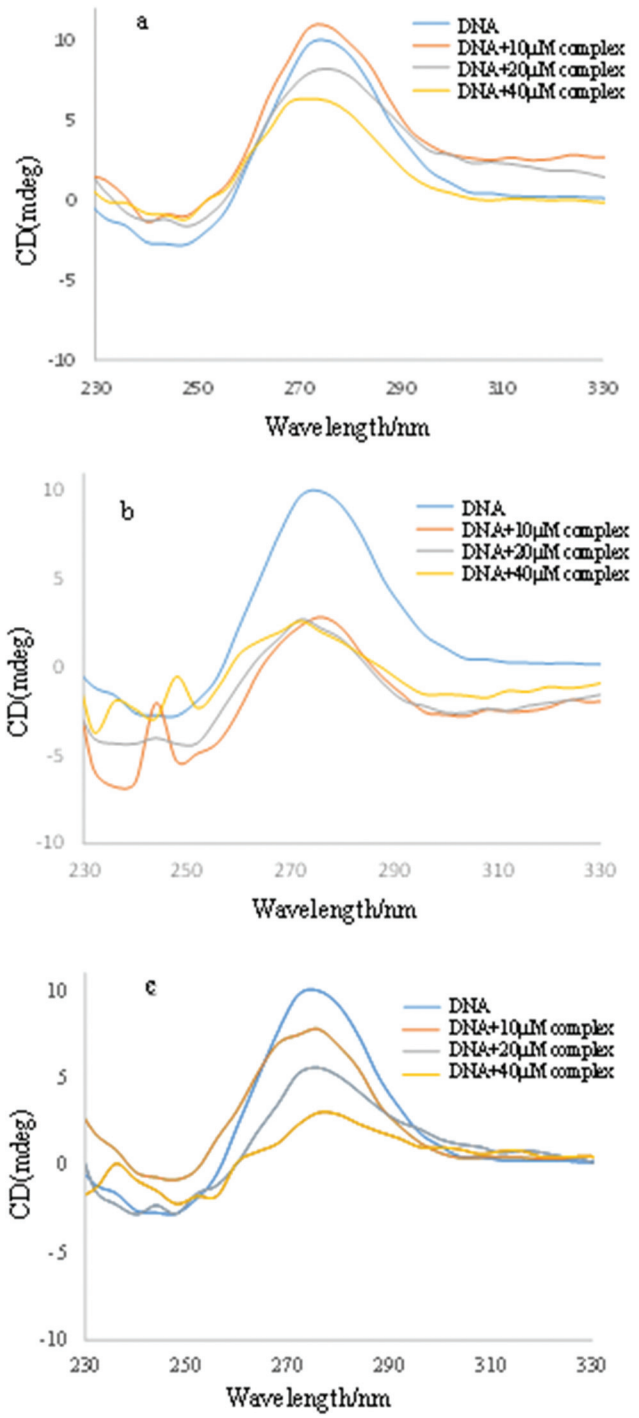

Fig. 5 CD spectra of DNA (200 μM) at increasing complexes concentration (0–40 μM) in buffer (1.0 mM Tris-HCl, 5 mM NaCl); (a) complex **1** (1000 μM); (b) complex **3** (1000 μM), (c) complex **5** (100 μM).

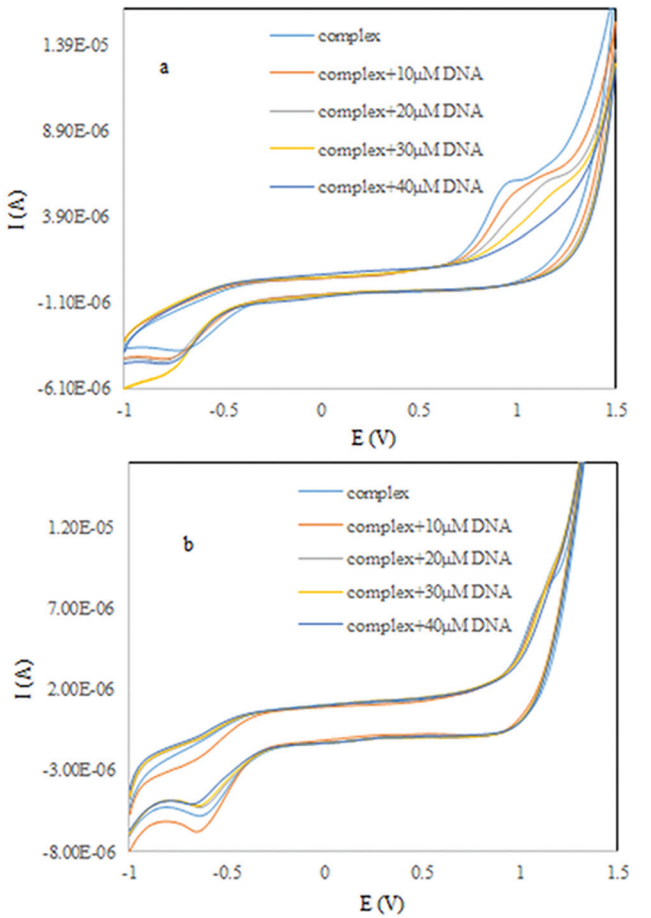

Fig. 6 Cyclic voltammograms of the complex: (a) complex **1** (1000 μM), (b) complex **2** (1000 μM) in the absence (**1**) and in the presence of (**2–5**) of DNA (10 μL, 10^4 μM in each injection) at 25.0 °C at 50 mV s^{-1} scan rate in 2% DMSO/1 mM Tris HCl/5 mM NaCl at pH 7.2.

complex (**1**) shows an anodic peak at 0.987 V and a cathodic peak at −0.641 V. With the increase in concentration of DNA (10 μL, 10^4 μM in each injection) in a constant amount of the complex (10 mL, 10^{-3} M), the voltammetric response of the compound changed as is evidenced by the sequential drop in peak current and, the cathodic potential Epc shows a positive shift while the anodic potential Epa shifts to negative values. These shifts of the potentials display that complex **1** can bind to DNA by both intercalation and electrostatic interactions.[110] The observed decrease in both the anodic and cathodic currents, suggest the binding of the complexes to the large gradually diffusing DNA molecule.[111] Further addition of FS-DNA (0.2–1.0 μM) led to the disappearance of the oxidative waves. The same result for complex **2** was observed.

In the absence of DNA, complex (**3**) shows an anodic peak at 1.136 V and a cathodic peak at −0.599 V (Fig. 6b). With the increase in concentration of DNA (10 μ, 10^4 μM in each injection) in a constant amount of the complex (10 mL, 10^3 μM), the voltammetric response of the compound changed as is evidenced by the sequential drop in peak current and gradual peak potential shift in the positive direction at both cathodic and anodic peaks that suggests the intercalation of complex **3** into DNA. The observed decrease in both the anodic and cathodic currents, suggests the binding of the complexes to the large slowly diffusing DNA molecule.[111] The same result for complex **4** was observed.

Fluorescence studies

To further confirm the interaction between the compounds and DNA, emission experiments were carried out. Ni and Zn complexes and the ligand show fluorescence at room temperature in solution or in the presence of FS-DNA, and their binding to DNA can be directly predicted through the emission spectra.

Thus, competitive EB binding studies can be ruled out.[112] In the case of intercalating drugs, the molecules are inserted into the base stack of the helix. The rotation of the free molecules prefers the radiationless deactivation of the excited states, but if the drugs are bound to DNA the deactivation through fluorescence emission is favored, and a significant increase in the fluorescence emission is generally observed. In the case of groove binding factors, electrostatic, hydrogen bonding or hydrophobic interactions are engaged and the molecules are close to the sugar-phosphate backbone, it being possible to detect a decrease in the fluorescence intensity in the presence of DNA.[113] Fluorescence emission is very sensitive to the situation, and therefore the fluorophore transfer from high to low polarity environments usually causes spectral shifts (10–20 nm) in the excitation and emission spectra of drugs.[114]

For Zn(II) complexes and the ligand with increasing concentrations of DNA, the intensity of the fluorescence spectra emission band at a maximum wavelength of about 498 nm obviously decreased and at about 445 nm slightly enhanced. Complex **1**, which bound to DNA more strongly, is more efficient than complex **2** in quenching emission because of its size.

Quenching of ligand and Zn(II) complexes bound to DNA is in good agreement with the linear Stern–Volmer equation.[115]

$$\frac{F_0}{F} = 1 + K_{SV}[Q] = 1 + k_q\tau_0[Q] \quad (4)$$

where F_0 and F are the steady-state fluorescence intensities in the absence and presence of a quencher, respectively. K_{SV} is the Stern–Volmer quenching constant and [Q] is the concentration of the quencher (DNA). The bimolecular quenching rate constant is k_q and the lifetime of the fluorophore is τ_o in the absence of the quencher (DNA). Since the fluorescence lifetime is naturally near 10^{-8} s, the bimolecular quenching constant (k_q) is calculated from $K_{sv} = k_q\tau_o$.[115] The fluorescence quenching curve of the complex by FS-DNA (Fig. 6) illustrates good agreement with the linear curve of the Stern–Volmer equation and K_{sv} is calculated by the ratio of the slope to the intercept (Table 2). The moderately large value of K_{sv} indicates that the **L**, complexes **1** and **2** are bound to DNA. According to eqn (4), k_q is greater than the limiting diffusion rate constant (2.0×10^{10} M^{-1} s^{-1}) for a biomacromolecule, indicating the existence of a static quenching mechanism. In the static quenching mechanism, the fluorophore and the quencher form a complex in the ground state.

The Ni(II) complexes can emit fluorescence in Tris-HCl buffer at ambient temperature with maxima appearing at about 450 nm. As shown in Fig. 7, the fluorescence intensities of the complexes are increased with increasing concentration of FS-DNA, which agrees with those observed for other intercalators[101] and confirms their interaction with FS-DNA.

Table 2 The Stern–Volmer quenching constant for the interactions of L and complexes **1**, **2** and K_f of them with DNA at 37 °C

Compound	K_{sv}[a]	k_q
L	1434.3	1.4×10^{11}
1	4040.6	4.0×10^{11}
2	409.0	4.0×10^{10}

[a] K_{SV} is obtained from the slope of the straight line.

This hints that the complexes can be inserted between DNA base pairs deeply and that they can bind to DNA. The binding of the complexes to DNA leads to an obvious increase in emission intensity which is also observed with complexes containing ligands bearing NH and OH groups.[100,116] This is due to the hydrophobic environment inside the DNA helix reducing the approachability of the solvent molecules as well as limiting the mobility of the complex at the binding site, which causes a reduction of the vibrational modes leading to a higher emission intensity.[117]

These fluorescence improvements exhibit that the complex interacted with DNA and their quantum efficiency was increased.

Like the quenching process, the enhancement constant can be obtained by eqn (5)[118]

$$\frac{F_0}{F} = 1 - K_E[E] \quad (5)$$

The enhancement constants of Ni(II) complex were calculated using eqn (5) (Fig. 7 and Table 3).

To determine the strength of the interaction of complexes with DNA, the value of the binding constant (K_f) resulted from the Scatchard equation:[119]

$$\log\left(\frac{F_0 - F}{F}\right) = \log K_f + n\log[DNA] \quad (6)$$

where F_0 and F are the fluorescence intensities of the fluorophore in the absence and in the presence of different concentrations of DNA, respectively and n is the number of binding sites.

The values of K_f for **L**, **1**, **2** were found to be 1.89×10^3 M^{-1}, 36.90×10^3 M^{-1} and 3.78×10^2 M^{-1}, and n = 1.02, 1.25, 0.99 respectively.

In the case of Ni(II) complexes, the emission intensity was enhanced, that is $F_0 < F$, and the titled equation becomes:[118]

$$\log\left(\frac{F - F_0}{F}\right) = \log K_f + n\log[DNA] \quad (7)$$

The values of K_f for **3**, **4**, **5** were found to be 3.26×10^2 M^{-1}, 2.91×10^2 M^{-1} and 4.59×10^2 M^{-1} and n = 0.76, 0.81, 0.81 respectively.

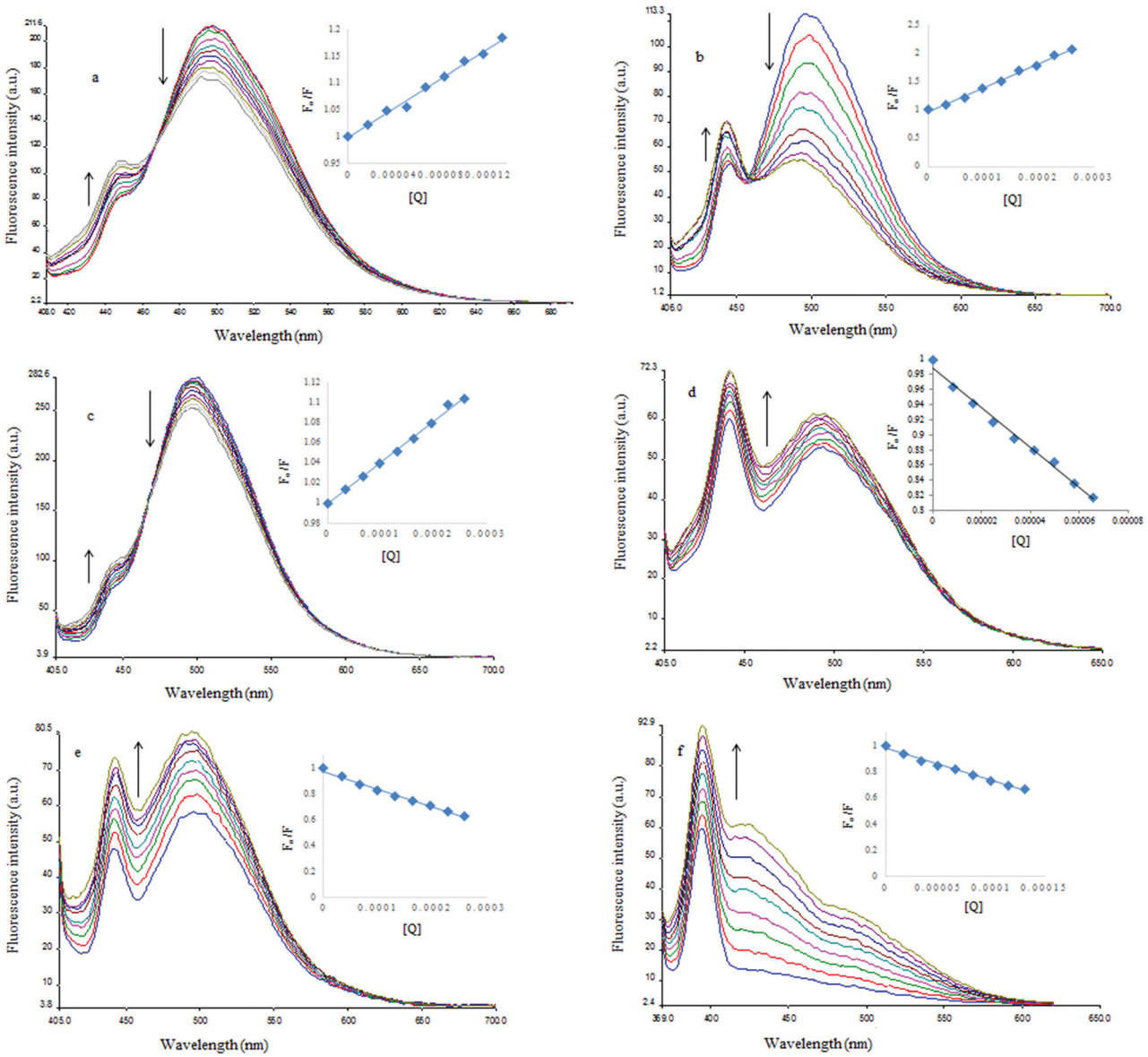

Fig. 7 (a–f) Effect of FS-DNA (0–260 μM in **1**, **2**, **4** and 0–65.8 μM in **3** and 0–132 μM in **L**, **5**) on the emission intensity of the **L** and **1–5** solution (1 μM). (Embedded) Stern–Volmer plot for the observed fluorescence of **L** and complexes upon the addition of DNA.

Table 3 Enhancement constants of complexes **3–5** with DNA at 37 °C

Complex	K_E
3	2645.5
4	1377.2
5	2480.7

K_E is obtained from the slope of the straight line.

The value of K_f clearly emphasizes the high affinity of compounds for DNA.

These results showed that the complexes bound more strongly than the free ligands. The higher binding affinity of the M(II) complexes is attributed to the extension of the π system of the intercalated ligand due to the coordination with the M(II) ion. Since the complexes have a greater planar area than that of the free ligand, the complexes penetrate more deeply into and stack more strongly with the base pairs of the DNA.

Gel electrophoresis study

Ligands with DNA interaction ability are always attractive due to their ability to cause numerous effects like gene expression modification, cell cycle arrest and DNA cleavage activity. Together or alone, these modifications change the fate of the cell to the special programmed cell death called apoptosis.

DNA cleavage including single or double strand breaks are mainly caused by ligands independently or with the contri-

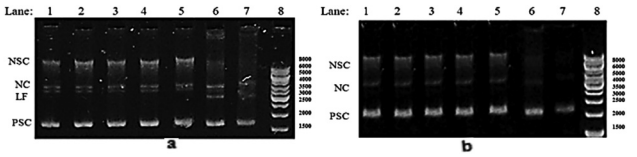

Fig. 8 Gel electrophoresis diagram of pBlu2KSM DNA in the presence of increasing amounts of (a) complex **3** and (b) complex **5** (lanes 1–7). Lane 1, DNA; lane 2, DNA + 30 μM ligand; lane 3, DNA + 40 μM ligand; lane 4, DNA + 50 μM ligand; lane 5, DNA + 60 μM ligand; lane 6, DNA + 70 μM ligand; lane 7, DNA + 80 μM ligand, lane 8; DNA ladder. Linear form (LF), nicked circular (NC) and positive and negative supercoiled (SC) of DNA are labeled, respectively.

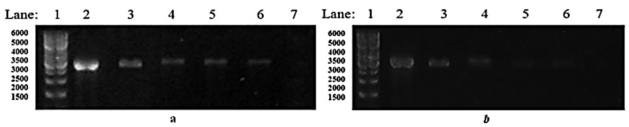

Fig. 9 Ethidium bromide displacement assay. Gel electrophoresis diagram of HindIII digested pBlu2KSM DNA in the presence of increasing amounts of (a) complex **3** and (b) complex **5**. Lane 1, DNA ladder; lane 2, DNA; lane 3, DNA + 50 μM ligand; lane 4, DNA + 60 μM ligand; lane 5, DNA + 70 μM ligand; lane 6, DNA + 80 μM ligand; lane 7, DNA + 90 μM ligand.

bution of oxidant factors like H_2O_2 and some intermediate elements like Cu^{2+} that are increased in the malignancy procedure. Among them double strand breaks cause the most harmful damage to the cells because cellular repair systems like NHEJ (Non-Homologous End Joining) almost always repair the strands with very low accuracy and several strand insertion/deletions will occur that causes genome instability. Finally this phenomenon drives cells to apoptosis. In this manner, supercoiled (SC) plasmid pBlu2KSM DNA was incubated with varying concentrations of complexes to investigate their DNA cleavage ability. As shown in Fig. 8, although complexes **3** & **4** caused significant intercalatory effects and also site-specific double strand break in concentrations higher than 50 μM, only complex **5** showed a slight intercalatory effect. This phenomenon is related to the nature of nickel as a successful ligand in the interaction with DNA. Moreover at higher concentrations, there is a change in the electrophoretic mobility of the NC form eventually leading to condensation of DNA. As shown in Fig. 9, the process of DNA condensation seems to start above 50 μM in **3** & **4** and 60 μM of **5** ligand concentrations. Ethidium bromide is introduced as a classical double strand DNA intercalator to investigate the affinity of ligands to attach to the DNA. To further confirm the interaction modes and affinity of the complex **3** with DNA, experiments on the competitive binding behavior of EB and compound **3** to DNA were carried out. HindIII digested plasmids in the presence of an increasing amount of complex **3** (lanes 3–7) were prepared and EB introduced as a control for classic intercalative interaction.

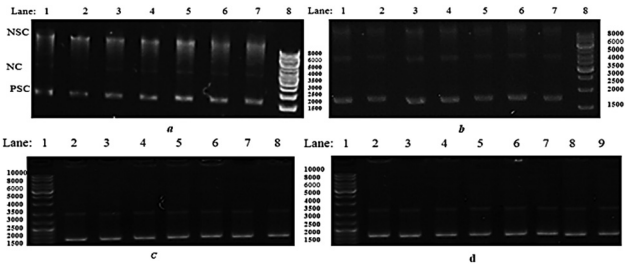

Fig. 10 Gel electrophoresis diagram of pBlu2KSM DNA in the presence of increasing amounts of (a) complex **1**, (b) complex **1** + H_2O_2, (c) complex **2** and (d) complex **2** + H_2O_2. (a and c): Lane 1, DNA Ladder; lane 2, DNA; lane 3, DNA + 30 μM ligand; lane 4, DNA + 40 μM ligand; lane 5, DNA + 50 μM ligand; lane 6, DNA + 60 μM ligand; lane 7, DNA + 70 μM ligand, lane 8; DNA + 80 μM ligand. (b and d): Lane 1, DNA; Lane 2, DNA + H_2O_2; lane 3, DNA + 30 μM ligand + H_2O_2; lane 3, DNA + 40 μM ligand + H_2O_2; lane 4, DNA + 50 μM ligand + H_2O_2; lane 5, DNA + 60 μM ligand + H_2O_2; lane 6, DNA + 70 μM ligand + H_2O_2; lane 7, DNA + 80 μM ligand + H_2O_2, lane 8; DNA ladder. Linear form (LF), nicked circular (NC) and positive and negative supercoiled (SC) of DNA are labeled, respectively.

According to Fig. 9, at concentrations higher than 50 μM, ethidium bromide displacement is started by complex **3** and the DNA band disappeared with no significant migration of the band. These results suggested the fact that the ethidium bromide replacement ability of the ligand is stronger than the twisting ability. The results may predict the complex **3** mode of action that like ethidium bromide could intercalate between DNA double strands causing insertion mutations and subsequently affect DNA replication and transcription.[92]

Although compound **1** has strong DNA binding affinity based on fluorescence studies, different concentrations of compounds **1** and **2** alone and in the presence of H_2O_2 doesn't show any intercalatory effects and single or double strand breaks (Fig. 10).

Cell viability

The ability of the drugs to induce either apoptosis or necrosis seems to be a primary factor in determining their anticancer efficacy. Successful anticancer drugs usually trigger several cellular mechanisms for killing the cells. These include DNA replication interfering (alkylating, antimetabolites and DNA-binding) agents, protein mimetics, cytostatic behaviour and energy producing starvation.[120,121] Additionally, the other pharmacodynamic factors like solubility, interactions with other biomolecules can affect the therapeutic properties of the drug.[122]

According to Table 4, the anticancer activities of Ni(II) and Zn(II) complexes toward human HepG2 and HeLa cancer cell lines have been examined in comparison with the currently used drug 5-fluorouracil under similar conditions by using the MTT assay. It is found that the compounds exhibit significant cytotoxic activities in a time-dependent manner in the range of 0–26 μM in 24 hours of incubation compared to the generally used 5-fluorouracil. Moreover, both nano-sized complexes

Table 4 Comparative IC_{50} values of Ni(II) and Zn(II) complexes when tested on HepG2 and HeLa cell lines after 24 and 48 hours

	HepG2		HeLa	
Complexes	24 h	48 h	24 h	48 h
1	7.3 ± 0.9[a]	4.6 ± 0.4	6.8 ± 0.7	4.7 ± 0.3
2	10.9 ± 1.8	8.7 ± 0.2	10.3 ± 1.5	9.1 ± 0.4
3	16.3 ± 0.6	11.7 ± 0.5	15 ± 1.7	11.2 ± 1.6
4	23.6 ± 0.4	18.9 ± 1.8	24.7 ± 1.1	20.6 ± 0.7
5	25.9 ± 1.3	21.1 ± 1.4	22.4 ± 0.5	21.9 ± 2.2
5FU[b]	33.5 ± 2.9	25 ± 2.7	20.4 ± 1.2	15.8 ± 2.1

[a] IC_{50} = the concentration of drug required to inhibit the growth of 50% of the cancer cells (μM). [b] 5-Fluorouracil.

exhibited strong DNA binding and slightly more effective anticancer activity compared to classical ones. Although the DNA binding activity might be due to the enhanced interaction efficiency of the nano-sized complexes, the slight cellular toxicity differences are related to quite complicated factors that should be investigated. The cell viability assay of the complexes showed that the Zn(II) complexes are more effective than Ni(II) complexes, despite the weakness of compound **1** to break DNA strands. The putative mechanism of these anticancer Zn(II) complexes remains unclear and further analysis should be performed. It could be emphasized that these compounds probably activate different and various pathways to induce apoptosis processes in cells. The mechanism of apoptosis is complex and cells can lead to apoptosis due to various physiological and pathological conditions. Since the cell is a complex unit and has complexity in its responses to various signals or compounds, the lack of logical relationship between the strength of DNA binding and cytotoxicity potentials of the complexes would be explainable. According to the Ni(II) double strand breaking ability and knowing the fact that double strand breaks are very efficient in triggering specifically the mitochondria related apoptosis pathway, the appropriate cytotoxicity mechanism of compound **3** might be the main intrinsic pathway of apoptosis induced by DNA damage.[123] When the DNA damage is recognized by the repaired protein complexes, the fate of the cell is survival or death. In this regard the cell cycle should be arrested to repair the damage or programmed cell death including apoptosis, necrosis and autophagy will occur if the damage is strong enough. Although the Classical Non Homologous End Joining (C-NHEJ) repair system is introduced as the most effective and fast mechanism for double strand break repair, the mechanism is error prone with minimum end processing and cell death is the fate of most damaged cells.[62]

DFT study

The geometries of ligands and complexes involved in this study were optimized by using the GAUSSIAN 03 program. The DFT method with B3LYP functional, LANL2DZ basis set for metal centers and 6-311g* for other atoms was used. The electronic properties of all compounds including: total energy (TE), dipole moment (DM), atomic charge of transition metal, energies of frontier orbital (HOMO and LUMO) and the energy gap between HOMO and LUMO orbital were calculated. The optimized geometries of the ligands and complexes are shown in Fig. 11. Selected geometrical parameters including bond lengths, bond angles and other parameters for all compounds are listed in Tables 5 and 6. Results show that all of the bond lengths and bond angles are in the normal range.

Molecular docking simulation

Molecular docking simulations of the synthesized compounds and DNA were performed to explore more details on the ligand conformation and their orientations in the active site of the receptor.

The lowest-energy conformations show that all compounds approach the gap between DNA minor grooves mainly through the metal centers and oxygen groups on the Schiff base structures (Fig. 12, S27 and S29†). While no hydrogen bonding was detected for any of the ligands, steric interaction was determined to play a dominant role in binding of the ligands to the DNA. The steric interactions arise from the (3-formyl-4-hydroxybenzyl)triphenylphosphonium chloride template and specifically the phenyl rings. The ligands stretch inside the minor groove so that the positively charged atom *i.e.* the transition metal and phosphor atoms are located between the negative phosphate backbones of DNA to stabilize the ligands through electrostatic potentials.

From a detailed analysis of the docked structures, it appears that the metal complexes are close to the DNA structure from the metal center and the oxygen groups of the Schiff base ligand and as mentioned in the Experimental section the nature of the metal has a great influence on interaction mode. Furthermore, it has been observed that most of the minor groove binding docked compounds prefer AT DNA sequences rather than GC DNA sequences and this preferential binding leads to a better van der Waals' interaction between the drug molecules and DNA functional groups.[124] It appears that the Ni compounds approach the thymine base while the Zn compound is close to the adenine base in the DNA structure.

The DNA binding affinity of the complexes may be predicted from the binding scores. The calculated binding scores for all optimized compounds are in the range of −95.232 to −115.373 (Table 7). It should be pointed out that the above docking calculation did not take the intercalation into account, and the results only allow a prediction of the binding affinity and the sterically acceptable conformations of the complexes to DNA.

The modes of binding of the complexes with DNA obtained from molecular docking studies correlate well with the experimental findings.

Therefore, on the basis of Rerank Score results, complex **3** is found to be more efficient towards the DNA target as compared to the other complexes. The DNA binding potency follows the order of: **3** > **5** > **1** > **L** as supported by the experi-

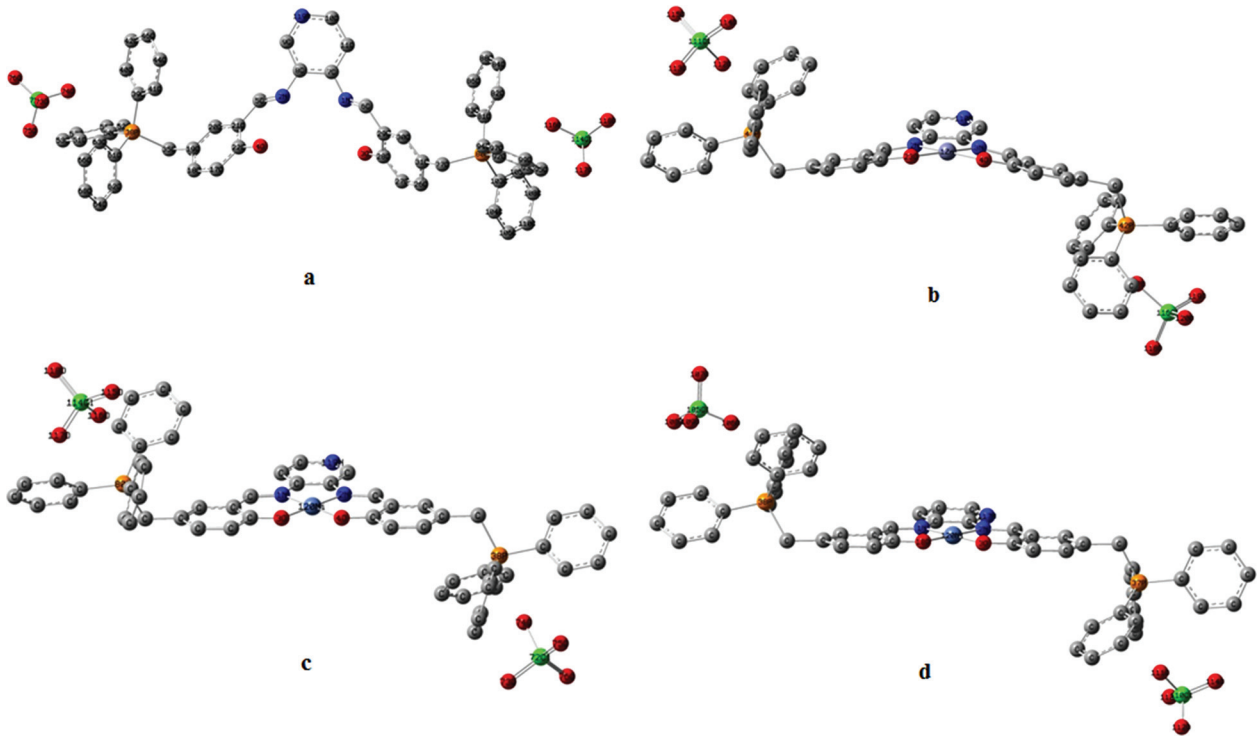

Fig. 11 The optimized geometrical structures of compounds: (a) free ligand, (b) [Zn(5-CH_2PPh_3-3,4-salpyr)]$(ClO_4)_2$ (**1**, **2**), (c) [Ni(5-CH_2PPh_3-3,4-salpyr)]$(ClO_4)_2$ (**3**, **4**), (d) [Ni(5-CH_2PPh_3-2,3-salpyr)]$(ClO_4)_2$ (**5**).

Table 5 Selected bond lengths in Å and angle (°) by theoretical calculation by the B3LYP method

Complex **5**		Complex **1**		Complex **3**	
Bond length					
Ni–N1	1.879	Zn–N2	2.126	Ni–N1	1.878
Ni–N2	1.877	Zn–N3	2.120	Ni–N2	1.863
Ni–O3	1.851	Zn–O4	1.951	Ni–O18	1.849
Ni–O4	1.849	Zn–O23	1.954	Ni–O3	1.848
Bond angles					
N1–Ni–N2	86.699	N2–Zn–N3	78.897	N1–Ni–N2	86.320
N1–Ni–O3	94.008	N3–Zn–O4	88.923	N1–Ni–O18	94.410
N2–Ni–O4	94.151	N2–Zn–O23	88.532	N2–Ni–O3	93.852
O3–Ni–O4	85.141	O4–Zn–O23	103.384	O3–Ni–O18	85.421
N1–Ni–O4	179.144	N2–Zn–O4	167.267	N2–Ni–O18	179.159
N2–Ni–O3	179.291	N3–Zn–O23	167.034	N1–Ni–O3	179.581

Table 6 The computed electronic properties of complexes by using theB3LYP method

	Complex **5**	Free ligand	Complex **1**	Complex **3**
E_{B3LYP} (a.u.)	−6226.00	−6227.182	−4783.298	−6227.182
μ (Debye)	10.125	4.567	1.021	4.567
HOMO (a.u.)	−0.234	−0.227	−0.245	−0.227
LUMO (a.u.)	−0.126	−0.112	−0.125	−0.112
HOMO–LUMO gap (eV)	2.936	3.135	3.253	3.135
Metal charge (mu)	1.206	1.032	1.241	1.032

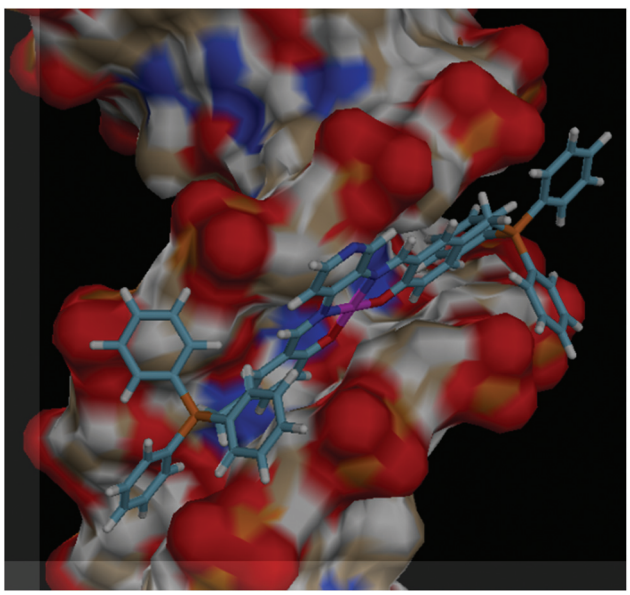

Fig. 12 Computational docking models (using the MVD software) illustrating the interactions between DNA and complex **3**.

mental finding. The results show the metal complexes act better than free ligand and Ni complexes, because of more planarity of their structures, are better than Zn complexes in their interaction with DNA.

Table 7 Docking results for binding scores of all the compounds to the DNA structures

Complex	Rerank score
Free ligand	−95.232
1	−100.827
3	−115.373
5	−105.471

Conclusions

The ligand (**L**) and new complexes have been synthesized and well characterized. The DNA binding properties of **L** and complexes **1–5** were examined by UV-Vis absorption spectra, emission spectra, viscosity, voltammetric techniques, and gel electrophoresis. The DNA binding properties of the free ligands and Zn(II) and Ni(II) complexes were investigated by absorption and fluorescence measurements. While **L** and complexes **1**, **2** interact with DNA, presumably by the groove binding mechanism, complexes **3–5** interacted with DNA through intercalation which was also confirmed by viscosity measurements and voltammetric techniques of DNA solutions in the presence of the complexes. The interaction occurrence is supported by the following findings:

I. Metal complexes strongly bind with DNA relative to the ligand.

II. Ni(II) complexes are better relative to Zn(II) complexes that may be attributed either to the z^* effect or geometry.

III. The size of particles influences interaction, so nano complexes bound to DNA are much stronger.

XI. Among the Ni(II) complexes: **3** > **4** > **5** and so complexes **3** & **4** containing 3,4-diaminopyridine as the bridging ligand interacted strongly with DNA relative to 2,3-diaminopyridine ones.

In the experiment on the DNA cleavage study by gel electrophoresis, the results showed that the double strand cleavage ability of compound **3** is viable for some time, while compounds **1** and **2** are able to cleave the DNA double strand helix in the presence and absence of H_2O_2. The cell viability assay showed the effective anticancer activity of all complexes, although the most effective complexes were of the Zn(II) complex family.

These nanocompounds are active for several reasons: it is a well-known fact that as their size gets smaller, their surface area-to-volume ratio increases. Therefore, as the nanoparticles are very small in size, they have an enormous surface area-to-volume ratio. The available surface areas of the active component of the nanoparticles are significant, which increase contact between the biomolecule such as DNA and these nanocompounds appreciably and helps to achieve a better reaction rate and higher efficiency.

Moreover, the DNA docking studies suggested that the free ligand binds with the nucleotide phosphate unit of the DNA backbone because of the $-CH_2-PPH_3^+$ group and all the metal complexes (Zn, Ni) interacted in the minor groove of DNA through the metal center and oxygen groups of the Schiff base ligand and prefer to bind to the AT DNA sequences rather than GC DNA sequences and this preferential binding leads to better van der Waals' interaction between the drug molecules and DNA functional groups.

The docking result also reveals the higher binding affinity of complex **3** towards DNA receptors in comparison with complexes **1** and the free ligand.

The main results of the present investigation confirmed that the introduction of various metal effects and the size of particles on these complexes can influence the DNA binding events and the *in vitro* anticancer activities, thus suggesting that the DNA binding ability and the anticancer activities may possibly be tuned through varying these factors in these compounds, which is useful for the design and synthesis of new metal-based drugs. The inherent properties of inorganic nanoparticles such as their platform-like surface modifications, surface to volume ratios, and unique optical and biological properties make them excellent candidates for future biomedical applications.

Acknowledgements

We are grateful to Shiraz University Research Council for its financial support.

References

1 A. Rajendran, C. J. Magesh and P. T. Perumal, *Biochim. Biophys. Acta*, 2008, **1780**, 282–288.
2 A. Arola-Arnal, J. Benet-Buchholz, S. Neidle and R. Vilar, *Inorg. Chem.*, 2008, **47**, 11910–11919.
3 B. Peng, W.-H. Zhou, L. Yan, H.-W. Liu and L. Zhu, *Transition Met. Chem.*, 2009, **34**, 231–237.
4 K. Takahashi, K. Fukiura, H. Arii and M. Chikira, *Nucleic Acids Symp. Ser.*, 2007, **51**, 189–190.
5 G.-D. Liu, J.-P. Liao, S.-S. Huang, G.-L. SHEN and R.-Q. YU, *Anal. Sci.*, 2001, **17**, 1031–1036.
6 G.-D. Liu, X. Yang, Z.-P. Chen, G.-L. Shen and R.-Q. Yu, *Anal. Sci.*, 2000, **16**, 1255–1259.
7 D. J. Gravert and J. H. Griffin, *Inorg. Chem.*, 1996, **35**, 4837–4847.
8 K. I. Ansari, J. D. Grant, G. A. Woldemariam, S. Kasiri and S. S. Mandal, *Org. Biomol. Chem.*, 2009, **7**, 926–932.
9 G. A. Woldemariam and S. S. Mandal, *J. Inorg. Biochem.*, 2008, **102**, 740–747.
10 J. G. Muller, L. A. Kayser, S. J. Paikoff, V. Duarte, N. Tang, R. J. Perez, S. E. Rokita and C. J. Burrows, *Coord. Chem. Rev.*, 1999, **185**, 761–774.
11 S. Routier, J.-L. Bernier, M. J. Waring, P. Colson, C. Houssier and C. Bailly, *J. Org. Chem.*, 1996, **61**, 2326–2331.
12 B. Rosenberg and L. Vancamp, *Nature*, 1969, **222**, 385–386.

13 E. R. Jamieson and S. J. Lippard, *Chem. Rev.*, 1999, **99**, 2467–2498.
14 I. Meistermann, V. Moreno, M. J. Prieto, E. Moldrheim, E. Sletten, S. Khalid, P. M. Rodger, J. C. Peberdy, C. J. Isaac and A. Rodger, *Proc. Natl. Acad. Sci. U. S. A.*, 2002, **99**, 5069–5074.
15 M. J. Bloemink, J. Reedijk, in *Metal Ions in Biological Systems*, ed. A. Sigel and H. Sigel, Marcel Dekker, Inc., New York, 1996, vol. 32, pp. 641–685.
16 K. E. Erkkila, D. T. Odom and J. K. Barton, *Chem. Rev.*, 1999, **99**, 2777–2796.
17 C. Metcalfe and J. A. Thomas, *Chem. Soc. Rev.*, 2003, **32**, 215–224.
18 R. B. Nair, E. S. Teng, S. L. Kirkland and C. J. Murphy, *Inorg. Chem.*, 1998, **37**, 139–141.
19 M. Cusumano, M. L. Di Pietro, A. Giannetto and P. A. Vainiglia, *J. Inorg. Biochem.*, 2005, **99**, 560–565.
20 A. Juris, V. Balzani, F. Barigelletti, S. Campagna, P. L. Belser and A. Von Zelewsky, *Coord. Chem. Rev.*, 1988, **84**, 85–277.
21 F. Meyer and H. Kozlowski, in *Comprehensive Coordination Chemistry II*, ed. J. A. M. J. Meyer, Pergamon, Oxford, 2003, pp. 247–554, DOI: 10.1016/B0-08-043748-6/05084-2.
22 H. Vahrenkamp, *J. Chem. Soc., Dalton Trans.*, 2007, 4751–4759.
23 H. Tapiero and K. D. Tew, *Biomed. Pharmacother.*, 2003, **57**, 399–411.
24 W. Maret, *BioMetals*, 2011, **24**, 411–418.
25 M. Alexiou, I. Tsivikas, C. Dendrinou-Samara, A. A. Pantazaki, P. Trikalitis, N. Lalioti, D. A. Kyriakidis and D. P. Kessissoglou, *J. Inorg. Biochem.*, 2003, **93**, 256–264.
26 R. Kurtaran, L. T. Yıldırım, A. D. Azaz, H. Namli and O. Atakol, *J. Inorg. Biochem.*, 2005, **99**, 1937–1944.
27 R. del Campo, J. J. Criado, E. García, M. A. R. Hermosa, A. Jimenez-Sanchez, J. L. Manzano, E. Monte, E. Rodrıguez-Fernández and F. Sanz, *J. Inorg. Biochem.*, 2002, **89**, 74–82.
28 W. Luo, X. Meng, X. Sun, F. Xiao, J. Shen, Y. Zhou, G. Cheng and Z. Ji, *Inorg. Chem. Commun.*, 2007, **10**, 1351–1354.
29 Z. Afrasiabi, E. Sinn, W. Lin, Y. Ma, C. Campana and S. Padhye, *J. Inorg. Biochem.*, 2005, **99**, 1526–1531.
30 M. C. Rodrìguez-Argüelles, M. B. Ferrari, F. Bisceglie, C. Pelizzi, G. Pelosi, S. Pinelli and M. Sassi, *J. Inorg. Biochem.*, 2004, **98**, 313–321.
31 A. Buschini, S. Pinelli, C. Pellacani, F. Giordani, M. B. Ferrari, F. Bisceglie, M. Giannetto, G. Pelosi and P. Tarasconi, *J. Inorg. Biochem.*, 2009, **103**, 666–677.
32 M. Di Vaira, C. Bazzicalupi, P. Orioli, L. Messori, B. Bruni and P. Zatta, *Inorg. Chem.*, 2004, **43**, 3795–3797.
33 E. Ferrada, V. Arancibia, B. Loeb, E. Norambuena, C. Olea-Azar and J. P. Huidobro-Toro, *Neurotoxicology*, 2007, **28**, 445–449.
34 S. Emami, S. J. Hosseinimehr, S. M. Taghdisi and S. Akhlaghpoor, *Bioorg. Med. Chem. Lett.*, 2007, **17**, 45–48.
35 Q. Huang, Z. Pan, P. Wang, Z. Chen, X. Zhang and H. Xu, *Bioorg. Med. Chem. Lett.*, 2006, **16**, 3030–3033.
36 P. Lemoine, B. Viossat, N. H. Dung, A. Tomas, G. Morgant, F. T. Greenaway and J. R. Sorenson, *J. Inorg. Biochem.*, 2004, **98**, 1734–1749.
37 J. d'Angelo, G. Morgant, N. E. Ghermani, D. Desmaële, B. Fraisse, F. Bonhomme, E. Dichi, M. Sghaier, Y. Li and Y. Journaux, *Polyhedron*, 2008, **27**, 537–546.
38 Y. Yoshikawa and H. Yasui, *Curr. Top. Med. Chem.*, 2012, **12**, 210–218.
39 H. Murakami, H. Yasui and Y. Yoshikawa, *Chem. Pharm. Bull.*, 2012, **60**, 1096–1104.
40 H. Sakurai, Y. Yoshikawa and H. Yasui, *Chem. Soc. Rev.*, 2008, **37**, 2383–2392.
41 W. B. Júnior, M. S. Alexandre-Moreira, M. A. Alves, A. Perez-Rebolledo, G. L. Parrilha, E. E. Castellano, O. E. Piro, E. J. Barreiro, L. M. Lima and H. Beraldo, *Molecules*, 2011, **16**, 6902–6915.
42 A. Tarushi, X. Totta, C. P. Raptopoulou, V. Psycharis, G. Psomas and D. P. Kessissoglou, *J. Chem. Soc., Dalton Trans.*, 2012, **41**, 7082–7091.
43 P. F. Liguori, A. Valentini, M. Palma, A. Bellusci, S. Bernardini, M. Ghedini, M. L. Panno, C. Pettinari, F. Marchetti and A. Crispini, *J. Chem. Soc., Dalton Trans.*, 2010, **39**, 4205–4212.
44 B. S. Mendiguchia, D. Pucci, T. F. Mastropietro, M. Ghedini and A. Crispini, *J. Chem. Soc., Dalton Trans.*, 2013, **42**, 6768–6774.
45 E. Ebrahimi, A. Jarrahpour, N. Heidari, V. Sinou, C. Latour, J. M. Brunel, A. R. Zolghadr and E. Turos, *Med. Chem. Res.*, 2016, **25**, 247–262.
46 A. Jarrahpour, M. M. Doroodmand and E. Ebrahimi, *Tetrahedron Lett.*, 2012, **53**, 2797–2801.
47 K. K. Jain, *BMC Med.*, 2010, **8**, 83.
48 B. Y. Kim, J. T. Rutka and W. C. Chan, *N. Engl. J. Med.*, 2010, **363**, 2434–2443.
49 C. Burda, X. Chen, R. Narayanan and M. A. El-Sayed, *Chem. Rev.*, 2005, **105**, 1025–1102.
50 G. Lövestam, H. Rauscher, G. Roebben, B. Sokull Klüttgen, N. Gibson, J. Putaud and H. Stamm, *Considerations on a definition of nanomaterial for regulatory purposes*, Publications Office of the European Union, Luxembourg, 2010, DOI: 10.2788/98686, ISBN 978-92-79-16014-1.
51 J. A. Barreto, W. O'Malley, M. Kubeil, B. Graham, H. Stephan and L. Spiccia, *Adv. Mater.*, 2011, **23**, H18–H40.
52 X. Chen and S. S. Mao, *Chem. Rev.*, 2007, **107**, 2891–2959.
53 S. Guo and E. Wang, *Nano Today*, 2011, **6**, 240–264.
54 J. Jang, in *Emissive Materials Nanomaterials*, Springer, 2006, pp. 189–260.
55 X. Lu, C. Wang and Y. Wei, *Small*, 2009, **5**, 2349–2370.
56 M. S. Mauter and M. Elimelech, *Environ. Sci. Technol.*, 2008, **42**, 5843–5859.
57 J. L. West and N. J. Halas, *Annu. Rev. Biomed. Eng.*, 2003, **5**, 285–292.
58 H. L. Karlsson, *Anal. Bioanal. Chem.*, 2010, **398**, 651–666.

59 P. Drevenšek, N. P. Ulrih, A. Majerle and I. Turel, *J. Inorg. Biochem.*, 2006, **100**, 1705–1713.
60 I. D. Vilfan, P. Drevenšek, I. Turel and N. Poklar Ulrih, *Biochim. Biophys. Acta, Gene Struct. Expression*, 2003, **1628**, 111–122.
61 A. Głuszyńska, K. Bajor, I. Czerwińska, D. Kalet and B. Juskowiak, *Tetrahedron Lett.*, 2010, **51**, 5415–5418.
62 M. Reichmann, S. Rice, C. Thomas and P. Doty, *J. Am. Chem. Soc.*, 1954, **76**, 3047–3053.
63 T. Mosmann, *J. Immunol. Methods*, 1983, **65**, 55–63.
64 S. P. Lees-Miller, *PLoS Genet.*, 2014, **10**, 1–3.
65 A. D. Becke, *J. Chem. Phys.*, 1993, **98**, 5648–5652.
66 M. J. Frisch, G. W. Trucks, H. B. Schlegel, G. E. Scuseria, M. A. Robb, J. R. Cheeseman, J. A. Montgomery, Jr., T. Vreven, K. N. Kudin, J. C. Burant, J. M. Millam, S. S. Iyengar, J. Tomasi, V. Barone, B. Mennucci, M. Cossi, G. Scalmani, N. Rega, G. A. Petersson, H. Nakatsuji, M. Hada, M. Ehara, K. Toyota, R. Fukuda, J. Hasegawa, M. Ishida, T. Nakajima, Y. Honda, O. Kitao, H. Nakai, M. Klene, X. Li, J. E. Knox, H. P. Hratchian, J. B. Cross, V. Bakken, C. Adamo, J. Jaramillo, R. Gomperts, R. E. Stratmann, O. Yazyev, A. J. Austin, R. Cammi, C. Pomelli, J. W. Ochterski, P. Y. Ayala, K. Morokuma, G. A. Voth, P. Salvador, J. J. Dannenberg, V. G. Zakrzewski, S. Dapprich, A. D. Daniels, M. C. Strain, O. Farkas, D. K. Malick, A. D. Rabuck, K. Raghavachari, J. B. Foresman, J. V. C. Ortiz, Q. A. G. Baboul, S. Clifford, J. Cioslowski, B. B. Stefanov, G. Liu, A. Liashenko, P. Piskorz, I. Komaromi, R. L. Martin, D. J. Fox, T. Keith, M. A. Al-Laham, C. Y. Peng, A. Nanayakkara, M. Challacombe, P. M. W. Gill, B. Johnson, W. Chen, M. W. Wong, C. Gonzalez and J. A. Pople, *Gaussian 03, revision C. 02*, 2004.
67 C. Chen, N. Gorlatova and O. Herzberg, *J. Biol. Chem.*, 2012, **287**, 7477–7486.
68 F. Keshavarz and D. Mohammad-Aghaie, *Phys. Chem. Res.*, 2015, **3**, 125–143.
69 R. Thomsen and M. H. Christensen, *J. Med. Chem.*, 2006, **49**, 3315–3321.
70 M. A. Lie, R. Thomsen, C. N. Pedersen, B. Schiøtt and M. H. Christensen, *J. Chem. Inf. Model.*, 2011, **51**, 909–917.
71 A. Satheshkumar and K. P. Elango, *Spectrochim. Acta, Part A*, 2014, **130**, 337–343.
72 R. Prabhakaran, R. Karvembu, T. Hashimoto, K. Shimizu and K. Natarajan, *Inorg. Chim. Acta*, 2005, **358**, 2093–2096.
73 P. Kalaivani, R. Prabhakaran, F. Dallemer, P. Poornima, E. Vaishnavi, E. Ramachandran, V. V. Padma, R. Renganathan and K. Natarajan, *Metallomics*, 2012, **4**, 101–113.
74 R. Prabhakaran, S. Anantharaman, M. Thilagavathi, M. Kaveri, P. Kalaivani, R. Karvembu, N. Dharmaraj, H. Bertagnolli, F. Dallemer and K. Natarajan, *Spectrochim. Acta, Part A*, 2011, **78**, 844–853.
75 H.-D. Yin, Q.-B. Wang and S.-C. Xue, *J. Organomet. Chem.*, 2004, **689**, 2480–2485.
76 Y.-L. Zhang, W.-J. Ruan, X.-J. Zhao, H.-G. Wang and Z.-A. Zhu, *Polyhedron*, 2003, **22**, 1535–1545.
77 G. Deacon and R. Phillips, *Coord. Chem. Rev.*, 1980, **33**, 227–250.
78 K. Nakamoto, *Infrared and Raman spectra of inorganic and coordination compounds*, Wiley Online Library, 1986.
79 Z.-C. Liu, B.-D. Wang, Z.-Y. Yang, Y. Li, D.-D. Qin and T.-R. Li, *Eur. J. Med. Chem.*, 2009, **44**, 4477–4484.
80 Z.-C. Liu, B.-D. Wang, B. Li, Q. Wang, Z.-Y. Yang, T.-R. Li and Y. Li, *Eur. J. Med. Chem.*, 2010, **45**, 5353–5361.
81 P. Krishnamoorthy, P. Sathyadevi, A. H. Cowley, R. R. Butorac and N. Dharmaraj, *Eur. J. Med. Chem.*, 2011, **46**, 3376–3387.
82 V. M. Manikandamathavan, R. P. Parameswari, T. Weyhermüller, H. R. Vasanthi and B. U. Nair, *Eur. J. Med. Chem.*, 2011, **46**, 4537–4547.
83 W. J. Mei, J. Liu, K. C. Zheng, L. J. Lin, H. Chao, A. X. Li, F. C. Yun and L. N. Ji, *J. Chem. Soc., Dalton Trans.*, 2003, 1352–1359.
84 R. K. Gupta, R. Pandey, G. Sharma, R. Prasad, B. Koch, S. Srikrishna, P.-Z. Li, Q. Xu and D. S. Pandey, *Inorg. Chem.*, 2013, **52**, 3687–3698.
85 G. Pratviel, J. Bernadou and B. Meunier, *Adv. Inorg. Chem.*, 1998, **45**, 251–312.
86 N. Shahabadi, S. Kashanian, M. Khosravi and M. Mahdavi, *Transition Met. Chem.*, 2010, **35**, 699–705.
87 S. Smith, G. Neyhart, W. Kalsbeck and H. Thorp, *New J. Chem.*, 1994, **18**, 397–406.
88 M. T. Carter, M. Rodriguez and A. J. Bard, *J. Am. Chem. Soc.*, 1989, **111**, 8901–8911.
89 M. Cory, D. D. McKee, J. Kagan, D. Henry and J. A. Miller, *J. Am. Chem. Soc.*, 1985, **107**, 2528–2536.
90 A. Pyle, J. Rehmann, R. Meshoyrer, C. Kumar, N. Turro and J. K. Barton, *J. Am. Chem. Soc.*, 1989, **111**, 3051–3058.
91 K. Ghosh, P. Kumar, N. Tyagi, U. P. Singh, V. Aggarwal and M. C. Baratto, *Eur. J. Med. Chem.*, 2010, **45**, 3770–3779.
92 M. Waring, *J. Mol. Biol.*, 1965, **13**, 269–282.
93 T.-R. Li, Z.-Y. Yang, B.-D. Wang and D.-D. Qin, *Eur. J. Med. Chem.*, 2008, **43**, 1688–1695.
94 A. Tarushi, J. Kljun, I. Turel, A. A. Pantazaki, G. Psomas and D. P. Kessissoglou, *New J. Chem.*, 2013, **37**, 342–355.
95 A. Tarushi, C. P. Raptopoulou, V. Psycharis, A. Terzis, G. Psomas and D. P. Kessissoglou, *Bioorg. Med. Chem.*, 2010, **18**, 2678–2685.
96 S. Sallam and A. Abbas, *J. Lumin.*, 2013, **136**, 212–220.
97 X.-L. Wang, H. Chao, H. Li, X.-L. Hong, Y.-J. Liu, L.-F. Tan and L.-N. Ji, *J. Inorg. Biochem.*, 2004, **98**, 1143–1150.
98 Q.-L. Zhang, J.-G. Liu, J. Liu, G.-Q. Xue, H. Li, J.-Z. Liu, H. Zhou, L.-H. Qu and L.-N. Ji, *J. Inorg. Biochem.*, 2001, **85**, 291–296.
99 A. Jancsó, L. Nagy, E. Moldrheim and E. Sletten, *J. Chem. Soc., Dalton Trans.*, 1999, 1587–1594.

100 J. M. Kelly, A. B. Tossi, D. J. McConnell and C. OhUigin, *Nucleic Acids Res.*, 1985, **13**, 6017–6034.
101 S. Satyanarayana, J. C. Dabrowiak and J. B. Chaires, *Biochemistry*, 1992, **31**, 9319–9324.
102 J. G. Collins, T. P. Shields and J. K. Barton, *J. Am. Chem. Soc.*, 1994, **116**, 9840–9846.
103 J.-H. Tan, Y.-J. Lu, Z.-S. Huang, L.-Q. Gu and J.-Y. Wu, *Eur. J. Med. Chem.*, 2007, **42**, 1169–1175.
104 A. M. Nowicka, A. Kowalczyk, S. Sek and Z. Stojek, *Anal. Chem.*, 2012, **85**, 355–361.
105 P. U. Maheswari and M. Palaniandavar, *J. Inorg. Biochem.*, 2004, **98**, 219–230.
106 C. JMDAN, L. Lerman and J. Venable, *Nature*, 1972, **236**, 67–70.
107 S. Srinivasan, J. Annaraj and P. Athappan, *J. Inorg. Biochem.*, 2005, **99**, 876–882.
108 A. M. Leone, J. D. Tibodeau, S. H. Bull, S. W. Feldberg, H. H. Thorp and R. W. Murray, *J. Am. Chem. Soc.*, 2003, **125**, 6784–6790.
109 M. T. Carter and A. J. Bard, *J. Am. Chem. Soc.*, 1987, **109**, 7528–7530.
110 K. Jiao, Q. X. Wang, W. Sun and F. F. Jian, *J. Inorg. Biochem.*, 2005, **99**, 1369–1375.
111 N. Muhammad, A. Shah, S. Shuja, S. Ali, R. Qureshi, A. Meetsma and M. N. Tahir, *J. Organomet. Chem.*, 2009, **694**, 3431–3437.
112 S. Dhar, M. Nethaji and A. R. Chakravarty, *J. Inorg. Biochem.*, 2005, **99**, 805–812.
113 W.-Y. Li, J.-G. Xu, X.-Q. Guo, Q.-Z. Zhu and Y.-B. Zhao, *Spectrochim. Acta, Part A*, 1997, **53**, 781–787.
114 D. Suh and J. B. Chaires, *Bioorg. Med. Chem.*, 1995, **3**, 723–728.
115 J. R. Lakowicz, *Principles of fluorescence spectroscopy*, Springer Science & Business Media, 2013.
116 F. Arjmand, B. Mohani and S. Ahmad, *Eur. J. Med. Chem.*, 2005, **40**, 1103–1110.
117 S. S. Bhat, A. S. Kumbhar, P. Lönnecke and E. Hey-Hawkins, *Inorg. Chem.*, 2010, **49**, 4843–4853.
118 N. Shahabadi, S. Kashanian and F. Darabi, *DNA Cell Biol.*, 2009, **28**, 589–596.
119 X.-Z. Feng, Z. Lin, L.-J. Yang, C. Wang and C.-L. Bai, *Talanta*, 1998, **47**, 1223–1229.
120 B. Denny and H. Wansbrough, *XII-Biotech. J. Cancer Drugs*, 1995, 1–12.
121 A. Delbridge and A. Strasser, *Cell Death Differ.*, 2015, **22**, 1071–1080.
122 J. T. DiPiro, *Concepts in clinical pharmacokinetics*, ASHP, 2010.
123 B. Kaina, *Biochem. Pharmacol.*, 2003, **66**, 1547–1554.
124 R. Filosa, A. Peduto, S. Di Micco, P. de Caprariis, M. Festa, A. Petrella, G. Capranico and G. Bifulco, *Bioorg. Med. Chem.*, 2009, **17**, 13–24.

